

A Novel Lie Group-based Reliable IMM Estimation Method for SINS/GNSS/OD/NHC Integrated Navigation in Complex Environments

Siyuan Du, Yulong Huang, *Senior Member, IEEE*, Weisong Wen, *Member, IEEE*, Yonggang Zhang, *Senior Member, IEEE*

Abstract—In the field of autonomous driving, the micro-electromechanical systems (MEMS)-based vehicle navigation usually adopts multi-sensor integrated navigation to achieve high-precision positioning. However, due to the complex environments, the accuracy and reliability of navigation sensors may be significantly reduced. To address these challenges, the interacting multiple model (IMM)-based strapdown inertial navigation system/global navigation satellite system/odometer/non-holonomic constrain (SINS/GNSS/OD/NHC) integrated navigation is adopted. Unfortunately, due to the use of traditional state-space model (SSM), the existing IMM estimation methods often suffer from poor estimation consistency, and the mounting error angle will also make OD/NHC subfilter models affect estimation consistency during the interaction process. Moreover, complex environments lead to frequent model switching, and relying on inaccurate model probabilities may cause significant fluctuations in the subfilter outputs, thereby reducing estimation accuracy. In contrast, the proposed IMM estimation method constructs Lie group-based subfilter SSM, which improves estimation consistency. Additionally, the velocity-bias-based mounting error angle estimation method is proposed by using variational Bayesian (VB) techniques, which further refines the OD/NHC models in IMM. On the other hand, a dynamic likelihood adaptive mechanism (DLAM) is introduced to improve reliability and mitigate the negative effects of frequent switching. Simulation and field test results demonstrate that the proposed velocity-bias-based mounting error angle estimation method has fast convergence speed and high convergence accuracy. Additionally, the proposed Lie group-based reliable IMM estimation method has better accuracy and robustness in complex environments as compared to the existing IMM estimation methods.

Index Terms—Autonomous vehicle, integrated navigation, Lie group, interactive multiple model, mounting error angle, variational Bayesian

I. INTRODUCTION

In recent years, the rapid advancement of 5G-based internet of things (IOT) technology has significantly accelerated the development of autonomous vehicles. These vehicles rely on

This work was supported in part by the National Key Research and Development Program of China under Grant No. 2023YFB3906403, and in part by the National Natural Science Foundation of China under Grant Nos. 62373118 and 62173105, and in part by the Natural Science Foundation of Heilongjiang Province of China under Grant No. ZD2023F002. (Corresponding author: Yulong Huang.)

S. Du, Y. Huang and Y. Zhang are with the College of Intelligent Systems Science and Engineering, Harbin Engineering University, Harbin 150001, China (e-mail: dusy@hrbeu.edu.cn; heuedu@163.com; zhangyg@hrbeu.edu.cn).

W. Wen is with Department of Aeronautical and Aviation Engineering, Hong Kong Polytechnic University, Hong Kong (e-mail: Weisong.wen@polyu.edu.hk).



Fig. 1: Diagram of complex vehicle navigation environments.

multi-sensor fusion to recognize and understand the surrounding environment, while 5G technology enables efficient communication and real-time data transmission [1]. Furthermore, high-precision navigation and positioning are crucial for ensuring the safety and reliability of autonomous vehicles [2]. To achieve this, the strapdown inertial navigation system/global navigation satellite system (SINS/GNSS) integrated navigation has been typically employed to provide high-precision navigation and positioning [3]. The micro-electromechanical systems (MEMS)-based SINS has the advantage of autonomy but suffers from accumulated errors, while GNSS provides accurate velocity and position information to correct these errors. However, as shown in Fig. 1, in complex environments such as tunnels, canyons, urban areas, GNSS signals may experience outliers or intermittent outages, which could compromise navigation reliability [4].

To enhance the navigation accuracy in poor GNSS signal quality, the odometer (OD) and non-holonomic constraints (NHC) are commonly employed as external aids in autonomous vehicle navigation. As velocity sensor, the OD is highly independent and resistant to interference, making it in SINS/OD integrated navigation [5]–[7]. Additionally, when vehicles move without lateral sliding or vertical bouncing, the NHC condition is satisfied, enabling virtual velocity observation for navigation. However, the mounting error angle (MEA) between the inertial measurement unit (IMU) frame and the vehicle frame, as shown in Fig. 2, can introduce errors into the SINS/OD/NHC integrated navigation. Furthermore, in environments with sharp turns, speed bumps, or rough roads, wheel slip or rebound can cause significant fluctuations or errors in velocity measurements. To address uncertainties

and faults from environmental interference, the interacting multiple model (IMM)-based integrated navigation method is often employed [8], [9]. The advantage of IMM-based integrated navigation is that it can flexibly switch subfilter models according to different navigation scenarios, providing stronger adaptability in complex environments.

Despite the widespread use of IMM-based integrated navigation, several critical issues remain in complex environments:

1) Inconsistent and inaccurate subfilter state-space models:

In existing IMM estimation methods, subfilter state-space model (SSM) is typically constructed based on traditional state error variables, which compromises estimation consistency. Specifically, the inaccurate navigation states within the SSM degrade consistency during the interaction process. Additionally, for OD/NHC subfilters, the mounting error angles can introduce velocity biases in the non-forward direction, and these biases exacerbate the instability in complex environments. This instability propagates through the interaction process, further degrading the overall estimation consistency. Therefore, constructing a consistent and accurate SSM, as well as effectively estimating of mounting error angle, is crucial to improving IMM performance.

2) Frequent switching of inaccurate probability models:

In complex environments, excessive sensitivity of model probability updates to measurement changes can lead to incorrect assumptions about the applicability of the current model, causing frequent switching to other models. Furthermore, if subfilter models do not adequately capture the dynamic properties of innovations, their similarities may hinder model differentiation, likewise resulting in frequent switching between similar models. Both cases can cause instability in the final weighted output. Therefore, a reliable model probability update method is essential for maintaining stability and accuracy in IMM-based estimation in complex environments.

To address these challenges, this paper proposes a novel Lie group-based reliable IMM SINS/GNSS/OD/NHC integrated navigation method, which enhances the consistency of subfilter SSM and improves the reliability of model probability update. The proposed method redefines the existing subfilter SSM within the Lie group framework for the first time. Additionally, a velocity-bias-based mounting error angle estimation method is introduced by using the variational Bayesian (VB) approach to mitigate the impact of OD/NHC subfilters on IMM consistency. Specifically, the velocity bias vector and covariance are modeled as a normal-inverse Wishart (NIW) distribution, and the VB method estimates these parameters jointly [43]. Subsequently, the mounting error angle is derived from the estimated velocity bias. This approach significantly enhances IMM performance in complex environments by improving subfilter SSMs consistency and refining the OD/NHC subfilter. In addition, to mitigate the negative impact of frequent model switching in complex environments, this paper proposes a dynamic likelihood adaptive mechanism (DLAM)-based reliable IMM estimation method. First, the consistent subfilter interaction and update process are conducted within the Lie group framework. Then, the proposed DLAM extends traditional Gaussian likelihood method, which flexibly addresses uncertainty by dynamically adjusting the weights of the Gaus-

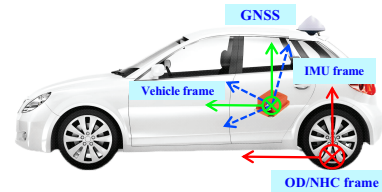


Fig. 2: The mounting error angle between IMU frame and vehicle frame.

sian and Student's t density functions. Specifically, when the Mahalanobis squared distance of the innovation vector exceeds the chi-square threshold, the Student's t weight is increased to enhance robustness, while under normal conditions, the Gaussian likelihood dominates to maintain precision. Finally, the final estimate is obtained by weighted fusion of the posterior estimates and updated model probabilities. The diagram of the proposed method is shown in Fig. 3. In conclusion, the contributions of this paper are as follows:

- To enhance IMM estimation consistency, the proposed method introduces consistent subfilter SSMs within Lie group framework for the first time. Then, a velocity-bias-based mounting error angle estimation method is proposed to refine the OD/NHC subfilter model. This method models the joint PDF of the velocity bias and its covariance matrix as a NIW distribution, using the estimated bias to indirectly calculate the mounting error angle.
- To enhance IMM estimation reliability, the DLAM-based model probability update method is proposed, which dynamically adjusts the weights between the Student's t and Gaussian likelihood functions based on the characteristics of the innovation vector, thereby improving the reliability of the IMM estimation method.
- Simulations and vehicle-mounted field experiments illustrate that the proposed velocity-bias-based mounting error angle demonstrates significant advantages in both convergence speed and accuracy. Additionally, in complex environments, the proposed novel Lie group-based IMM method for SINS/GNSS/OD/NHC integrated navigation is more accurate and reliable than the existing state-of-the-art methods.

The remainder of this paper is organized as follows. The related works are presented in Section II. The problem statement and motivations are given in Section III. In Section IV, a velocity-bias-based mounting error angle estimation method is proposed by VB method. In Section V, a novel Lie group-based reliable IMM method for SINS/GNSS/OD/NHC integrated navigation is proposed. In Sections VI and VII, through simulations and vehicle-mounted field tests, the performance of the proposed method is compared with that of existing state-of-the-art methods. Conclusions are drawn in Section VIII.

II. RELATED WORKS

A. Consistent integrated navigation estimation methods

To improve integrated navigation estimation consistency, recent methods have focused on the perspective of coordinate

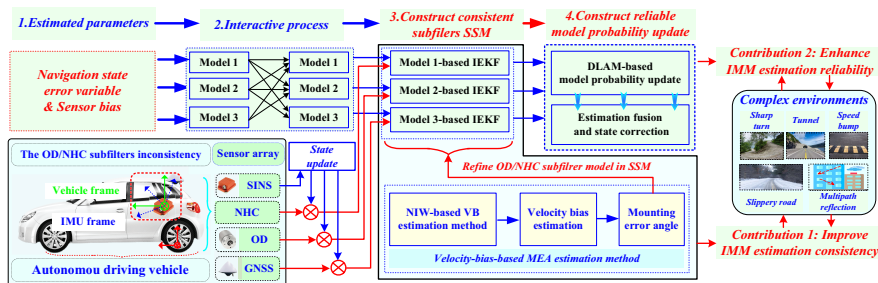


Fig. 3: Diagram of Lie group-based reliable IMM estimation method for SINS/GNSS/OD/NHC integrated navigation.

system transformation. Different coordinate system definitions lead to changes in the SINS state error equation and corresponding filtering SSMs. The traditional error-variable-based SSMs often ignore coordinate system incompatibilities, applying Euclidean space rules, which causes inconsistent estimates. Specifically, overestimation occurs when estimated error variance is smaller than the actual error variance, and conversely, underestimation occurs [10]. To address this, Crassidis *et al.* proposed a geometric extended Kalman filter (GEKF) based on common coordinate system [11], [12], which was later extended to a state-transformation extended Kalman filter (STEKF) [13]. The two methods redefine the velocity error variable, so the derived state-transition matrix can effectively alleviate the inconsistency caused by the force computation error. However, these methods still struggle to fully eliminate state dependencies, with inaccurate navigation states affecting estimation consistency. To further enhance estimation consistency, Barrau *et al.* proposed the Lie group-based invariant extended Kalman filter (IEKF) [14], which has been widely used in integrated navigation [15], leg-robot state estimation [16], and visual-inertial navigation [17]. The core idea of IEKF is to reconstruct the Lie algebra SSM through a group affine system, ensuring that the state-transition matrix is independent of inaccurate navigation states. Additionally, IEKF can be divided into left-invariant extended Kalman filter (LIEKF) and right-invariant extended Kalman filter (RIEKF) [15], with LIEKF being suitable for GNSS/NHC-based integration [18] and RIEKF better for OD-based integration [20]. Furthermore, IEKF-based integrated methods have been applied to various frames (*i*, *e*, and *n* frames) [19]–[21], with the *n*-frame being intuitive and suitable for MEMS-based navigation. As a further application of Lie group theory, the Lie group-based unscented Kalman filter (LGUKF) captures nonlinear state propagation using invariant error sigma-points [22]–[24], but it comes with a higher computational cost compared to IEKF, especially in multi-subfilters.

In conclusion, the existing Lie group-based consistent estimation methods mainly focus on single measurement model, which uses a unified approach for all types of measurements. In contrast, the research on multi-model fusion methods within the Lie group framework is still limited. Especially in IMM estimation methods, the consistency advantage of Lie group-based methods has not been fully utilized. Therefore, this paper proposes an LIEKF-based IMM estimation method within the *n* frame to improve the estimation consistency in

complex environments.

B. Mounting error angle estimation methods

As a commonly used navigation sensor, OD provides stable position measurements during GNSS outages. Compared to visual odometry and lidar, OD offers advantages such as low cost, insensitivity to light, and independence from environmental features. Meanwhile, the NHC is used to correct OD measurements and enhance navigation accuracy [25]. To optimize OD/NHC performance, the mounting error angle must be accurately determined. The existing mounting error angle estimation methods can be categorized into acceleration-based [26], velocity-based [27], and position-based [28]. The acceleration and velocity-based methods calculate the mounting error angle indirectly through the projection deviation of the SINS in the horizontal and vertical directions. However, these methods are sensor-dependent, making them less suitable for MEMS-based SINS. Additionally, the estimated mounting error angle will be coupled with inaccurate navigation states, thereby affecting the estimation accuracy. In contrast to other methods, the position-based observation method has higher estimation accuracy, but its inherent "off-line" and heavily reliant on posterior state estimates may reduce the estimation accuracy of mounting error angle [28]. To improve estimation accuracy, this paper proposes a novel velocity-bias-based mounting error angle estimation method. Unlike existing methods, the proposed method estimates the velocity bias and decouples the error angle from the navigation state. Additionally, as vehicle speed increases, the estimated velocity bias also increases, which will benefit the proposed NIW-based VB estimation.

C. IMM-based integrated navigation estimation methods

To achieve high-precision navigation in complex environments, the centralized EKF (C-EKF) is widely used, but uncertain non-Gaussian noise can reduce the estimation accuracy. To address this, the robust adaptive estimation methods have been proposed, including Sage-Husa KF [29], maximum likelihood (ML)-based innovation KF [30], and fading factor-based KF [31]. Each has limitations: the Sage-Husa KF may not converge to the correct noise covariance, the ML-based KF requires large data, and the fading factor-based KF struggles with optimal factor determination. Additionally, the M-estimation-based robust KFs enhance outlier resistance but may suffer from poorly set cost functions [32], [33].

Furthermore, if the noise distribution is well modeled in the Bayesian framework, the state and parameters can be estimated jointly using VB method, which achieves higher accuracy [34]–[36].

These methods are essentially based on a unified framework for robust adaptive filtering in which all measurements are integrated into a single equation. While this improves system observability, the problems arise when the vehicle transitions from open areas to urban canyons or from stable roads to rugged terrain, as the filtering parameters take time to adjust. Additionally, the inaccuracies in sub-parameters can affect the overall performance. In contrast, the IMM-based estimation methods have attracted considerable attention due to their adaptive model selection capabilities [37]–[42]. For example, nonlinear filtering can be introduced to handle model errors, but it increases computational complexity and may lead to instability due to uncertainty noise [37]. To adapt the uncertainty noise, prior noise covariance matrices can be preset in subfilters, but this method is heavily dependent on the prior settings and requires extensive computation [38]. Although M-estimation can also be introduced into IMM to enhance outlier suppression [39], unreasonable set robust cost functions can cause inconsistencies and instability in model probability updates. In the VB-IMM framework, the PDF of noise covariance matrix can be finely modeled, and then the state vector, unknown scale matrix, and other related parameters are jointly estimated. For example, the unknown noise covariance matrix can be modeled as an inverse Wishart (IW) distribution and estimated by VB-IMM [40]. To address outliers noise, the Student's *t*-based Gaussian approximation filtering method is incorporated into IMM framework [41]. For the heavy-tailed or skewed noise, a skew Gaussian-Gamma mixture distribution-based IMM method is proposed [42]. However, the existing VB-IMM estimation method has the problems: First, it requires a large number of iterative calculation to infer the state and related parameters. Second, it is mainly applied to target tracking models, and its effectiveness in multi-sensor integrated navigation models has yet to be fully validated. Third, the Gaussian likelihood function-based model probability update may be overly sensitive to environmental changes, leading to estimation fluctuations, response delays, and even filter divergence. To ensure effective fusion of subfilter estimation, a consistent-accurate SSM-based IMM estimation method within the Lie group framework. Additionally, a DLAM-based reliable model probability update method is proposed, which maintains sensitivity to environmental changes without over-reacting. Section III will provide a detailed problem statement and motivation behind the proposed method.

III. PROBLEM STATEMENT AND MOTIVATIONS

To maximize OD/NHC potential, the mounting error angle between the IMU frame and the vehicle frame needs to be accurately estimated. Generally, the IMU frame is set as the body frame, and the velocity in body frame is formulated as

$$\mathbf{v}^b = \mathbf{C}_b^n \mathbf{v}^n \quad (1)$$

where $\mathbf{v}^b = [v_x^b, v_y^b, v_z^b]^T$ denotes the body velocity in right-front-up *b* frame, and \mathbf{C}_b^n denotes the attitude rotation matrix,

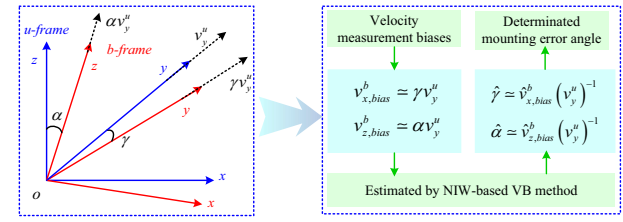


Fig. 4: The velocity biases induced by mounting error angle.

and \mathbf{v}^n denotes the velocity in navigation frame. However, the body frame is actually not aligned with vehicle frame, and then the velocity in vehicle frame is formulated as

$$\mathbf{v}^u = \mathbf{C}_b^u \mathbf{C}_n^b \mathbf{v}^n \quad (2)$$

where $\mathbf{v}^u = [v_x^u, v_y^u, v_z^u]^T$ denotes the vehicle velocity in right-front-up *u* frame. In addition, according to the criterion of NHC, the approximation is obtained as follows

$$v_x^u = v_z^u = 0 \quad (3)$$

and \mathbf{C}_b^u denotes the mounting error angle matrix, which can be approximated as follows

$$\mathbf{C}_b^u \approx \begin{bmatrix} 1 & -\gamma & \beta \\ \gamma & 1 & -\alpha \\ -\beta & \alpha & 1 \end{bmatrix} \quad (4)$$

where $[\alpha, \beta, \gamma]$ denote the mounting error angle of pitch, roll, and heading, respectively. Due to the lack of observability, the roll mounting error angle cannot be estimated. In order to estimate the mounting error angle $[\alpha, \gamma]$ effectively, this paper is motivated by the relationship between the mounting error angle and velocity bias. Consequently, substituting (4) into (2) yields as follows.

$$\begin{aligned} v_x^b &= v_x^u + \gamma v_y^u - \beta v_z^u \\ v_z^b &= v_z^u - \alpha v_y^u + \beta v_x^u \end{aligned} \quad (5)$$

where v_x^u and v_z^u are denoted in (3). It is evident that when the vehicle is moving at a constant velocity, the corresponding γv_y^u and αv_y^u will exhibit a constant velocity bias as follows.

$$\begin{aligned} v_{x,bias}^b &\simeq \gamma v_y^u \\ v_{z,bias}^b &\simeq \alpha v_y^u \end{aligned} \quad (6)$$

where the velocity biases $v_{x,bias}^b$ and $v_{z,bias}^b$ will not only break the NHC criterion, but also prevent OD from being in the optimal frame. Actually, if the constant velocity is larger, the velocity bias caused by the mounting error angle is also larger.

Motivated by the above analyses, if the velocity bias and constant vehicle velocity are known at a given time, the corresponding mounting error angle can be indirectly determined, as shown in Fig. 4. As a result, a velocity-bias-based mounting error angle estimation method is proposed. Specifically, the joint PDF of the velocity bias vector and its covariance matrix is modeled as as the NIW distribution by combining the properties of the multivariate normal and IW distributions. Then, the state vector, velocity bias vector, and covariance matrix are jointly estimated by VB method under the derived hierarchical Gaussian model. Subsequently, the mounting error angle is derived from the estimated velocity bias using (6).

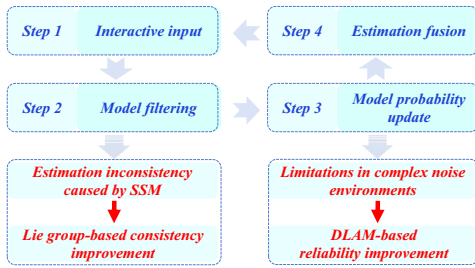


Fig. 5: Challenges and solutions to existing IMM methods.

Additionally, since only straight-line maneuver is required, the OD/NHC lever arm will not be coupled into the velocity bias through the turn rate, which means that the lever arm will not affect the estimation accuracy of the mounting error angle.

In IMM-based SINS/GNSS/OD/NHC integrated navigation, constructing consistent-accurate SSM is crucial for improving estimation accuracy. However, the existing IMM SSM is derived from traditional state error, and both the state model and the measurement model contain unknown navigation states, resulting in inconsistent estimation problem. This inconsistency directly affects convergence speed and accuracy, and inaccurate state interactions exacerbate the problem. Motivated by the advantages of Lie group theory in improving estimation consistency [19], [20], we propose the left-invariant error-based subfilter state model, and implement consistency improvements for NHC, OD, and GNSS. Compared to existing methods, this approach improves state independence and minimizes inter-filter influence. Additionally, the traditional IMM model probability update is typically assumed to follow a Gaussian distribution as follows [45].

$$\begin{cases} \Lambda_k^j = \frac{1}{(2\pi)^{d/2} |\mathbf{S}_k^j|^{1/2}} \exp \left\{ -\frac{1}{2} (\tilde{\mathbf{z}}_k^j)^T (\mathbf{S}_k^j)^{-1} \tilde{\mathbf{z}}_k^j \right\} \\ \boldsymbol{\mu}_k^j = \frac{\Lambda_k^j \sum_{i=1}^N \mathbf{p}^{ij} \boldsymbol{\mu}_{k-1}^i}{\sum_{j=1}^N \left(\Lambda_k^j \sum_{i=1}^N \mathbf{p}^{ij} \boldsymbol{\mu}_{k-1}^i \right)} \end{cases} \quad (7)$$

where Λ_k^j denotes the likelihood function value of model j at time k , and d denotes the dimension of measurement vectors, and N denotes the total number of models, and $\tilde{\mathbf{z}}_k^j$ and \mathbf{S}_k^j denote the measurement innovation vector and corresponding covariance matrix of model j at time k , respectively, and \mathbf{p}^{ij} denotes the transition probability from model i to model j , and $\boldsymbol{\mu}_k^{(j)}$ and $\boldsymbol{\mu}_{k-1}^{(i)}$ denote the model j probability at time k and model i probability at time $k-1$, respectively. However, in complex navigation environments, frequent model switching the relies on inaccurate likelihood values can lead to estimation errors. Specifically, extreme likelihood values may make IMM estimation methods unable to adapt quickly to environmental changes, resulting in inaccurate state estimates.

To address these issues, an direct heuristic idea is to improve the likelihood function hypothesis to better capture the characteristics of measurement innovation. Accordingly, we propose a reliable model probability update method based on the dynamic likelihood adaptive mechanism, which incorporates a Student's t likelihood function and Gaussian likelihood function. Additionally, the proposed method leverages the heavy-

tailed property of Student's t distribution to enhance robustness against outliers, and determines the weight of likelihood value by comparing the Mahalanobis squared distance of the innovation vector with the chi-square threshold. Specifically, if the distance exceeds the threshold, the Student's t likelihood weight is increased; otherwise, the Gaussian weight is increased. The weighted likelihood values are then normalized for model probability update. Fig. 5 illustrates the challenges and solutions in the existing IMM method. Sections IV and V provide a detailed discussion of the proposed methods.

IV. PROPOSED VELOCITY-BIAS-BASED MOUNTING ERROR ANGLE ESTIMATION METHOD

A. Lie group-based state-space model

In the inertial navigation, the attitude rotation matrix \mathbf{C} , velocity vector \mathbf{v} , and position vector \mathbf{r} actually belong to $SE_2(3)$, which is represented as follows [15], [23]

$$\mathbf{T} \triangleq \begin{bmatrix} \mathbf{C} \in SO(3) & \mathbf{v} \in \mathbb{R}^3 & \mathbf{r} \in \mathbb{R}^3 \\ \mathbf{0}_{1 \times 3} & 1 & 0 \\ \mathbf{0}_{1 \times 3} & 0 & 1 \end{bmatrix} \in SE_2(3) \quad (8)$$

For the definition of left invariant error $[\phi^b, \zeta_v^L, \zeta_r^L]$, it can be transformed from the left group error $\delta\mathbf{T}^L$, which is formulated as [15], [23]

$$\begin{aligned} \delta\mathbf{T}^L = \tilde{\mathbf{T}}^{-1}\mathbf{T} &= \begin{bmatrix} \tilde{\mathbf{C}}^T \mathbf{C} & \tilde{\mathbf{C}}^T(\mathbf{v} - \tilde{\mathbf{v}}) & \tilde{\mathbf{C}}^T(\mathbf{r} - \tilde{\mathbf{r}}) \\ \mathbf{0}_{1 \times 3} & 1 & 0 \\ \mathbf{0}_{1 \times 3} & 0 & 1 \end{bmatrix} \\ &= \begin{bmatrix} \exp_G(\phi^b \times) & \mathbf{J}(\phi^b) \zeta_v^L & \mathbf{J}(\phi^b) \zeta_r^L \\ \mathbf{0}_{1 \times 3} & 1 & 0 \\ \mathbf{0}_{1 \times 3} & 0 & 1 \end{bmatrix} \end{aligned} \quad (9)$$

where

$$\exp_G(\phi^b \times) \approx \mathbf{I}_3 + \phi^b \times \quad (10)$$

$$\mathbf{J}(\phi^b) \zeta_v^L = -\tilde{\mathbf{C}} \delta \mathbf{v} \quad (11)$$

$$\mathbf{J}(\phi^b) \zeta_r^L = -\tilde{\mathbf{C}} \delta \mathbf{r} \quad (12)$$

Similarly, the right invariant error $[\phi^n, \zeta_v^R, \zeta_r^R]$ can be transformed from the right group error $\delta\mathbf{T}^R$, which is formulated as [15], [23]

$$\begin{aligned} \delta\mathbf{T}^R = \mathbf{T}\tilde{\mathbf{T}}^{-1} &= \begin{bmatrix} \mathbf{C}\tilde{\mathbf{C}}^T & \mathbf{v} - \mathbf{C}\tilde{\mathbf{C}}^T\tilde{\mathbf{v}} & \mathbf{r} - \mathbf{C}\tilde{\mathbf{C}}^T\tilde{\mathbf{r}} \\ \mathbf{0}_{1 \times 3} & 1 & 0 \\ \mathbf{0}_{1 \times 3} & 0 & 1 \end{bmatrix} \\ &= \begin{bmatrix} \exp_G(\phi^n \times) & \mathbf{J}(\phi^n) \zeta_v^R & \mathbf{J}(\phi^n) \zeta_r^R \\ \mathbf{0}_{1 \times 3} & 1 & 0 \\ \mathbf{0}_{1 \times 3} & 0 & 1 \end{bmatrix} \end{aligned} \quad (13)$$

where

$$\exp_G(\phi^n \times) \approx \mathbf{I}_3 + \phi^n \times \quad (14)$$

$$\mathbf{J}(\phi^n) \zeta_v^R = -\delta \mathbf{v} + \tilde{\mathbf{v}} \times \phi^n \quad (15)$$

$$\mathbf{J}(\phi^n) \zeta_r^R = -\delta \mathbf{r} + \tilde{\mathbf{r}} \times \phi^n \quad (16)$$

Then, the state update equation of SINS with group affine system characteristics is given as follow [21]

$$\begin{aligned} \dot{\mathbf{C}}_b^n &= \mathbf{C}_b^n (\omega_{ib}^b \times) - (\omega_{in}^n \times) \mathbf{C}_b^n \\ \dot{\mathbf{v}}_{ib}^n &= -(\omega_{in}^n \times) \mathbf{v}_{ib}^n + \mathbf{C}_b^n \mathbf{f}_{ib} + \mathbf{G}^n \\ \dot{\mathbf{r}}_{ib}^n &= -(\omega_{in}^n \times) \mathbf{r}_{ib}^n + \mathbf{v}_{ib}^n \end{aligned} \quad (17)$$

where b , n , and i denote the body frame, local navigation frame, and inertial frame, respectively; \mathbf{C}_b^n denotes the attitude matrix from b to n ; \mathbf{v}_{ib}^n and \mathbf{r}_{ib}^n denote the projected velocity and position of b frame relative to the i frame in n frame, respectively; ω_{in}^n denotes the angular rate of n relative to i in n . ω_{ib}^b denotes the gyroscope angular rate, and \mathbf{f}_{ib}^b denotes the accelerometer specific force; \mathbf{G}^n denotes the gravitational force projected to n , and the relationship between gravitational force \mathbf{G}^n and gravity \mathbf{g}^n is as follows

$$\mathbf{G}^n = \mathbf{g}^n + (\omega_{ie}^n)^2 \mathbf{r}_{ib}^n \quad (18)$$

where ω_{ie}^n denotes the earth rotation rate in n . The gyroscope and accelerometer output models are given as follows

$$\begin{aligned} \omega_{ib}^b &= \tilde{\omega}_{ib}^b - \varepsilon^b - \sigma_{gyro} \\ \dot{\varepsilon}^b &= \mathbf{0} \end{aligned} \quad (19)$$

$$\begin{aligned} \mathbf{f}^b &= \tilde{\mathbf{f}}^b - \nabla^b - \sigma_{acc} \\ \dot{\nabla}^b &= \mathbf{0} \end{aligned} \quad (20)$$

where $\tilde{\omega}_{ib}^b$ and $\tilde{\mathbf{f}}^b$ denote the error contaminated angular rate and specific, respectively, ε^b and ∇^b are gyroscope constant bias and accelerometer constant bias, respectively, and σ_{gyro} and σ_{acc} are both zero-mean Gaussian white noise. Based on invariant error, the state models can be obtained as follows:

$$\mathbf{x}_{k|k-1}^L = \mathbf{F}_{k|k-1}^L \mathbf{x}_{k-1}^L + \mathbf{G}_{k-1}^L \mathbf{w}_b \quad (21)$$

where \mathbf{w}_b is assumed to be Gaussian distribution, i.e., $\mathbf{w}_b \sim N(\mathbf{0}, \mathbf{Q}_k)$ and $\mathbf{w}_b = [\mathbf{w}_{gyro}, \mathbf{w}_{acc}]^T$, and \mathbf{x}_{k-1}^L , \mathbf{F}_{k-1}^L , and \mathbf{G}_{k-1}^L denotes the left invariant error, left state transition matrix, and left state noise matrix, respectively. Subsequently, \mathbf{x}_{k-1}^L is given as follows.

$$\mathbf{x}_{k-1}^L = [\phi^b \quad \zeta_v^L \quad \zeta_r^L \quad \varepsilon_b \quad \nabla_b]^T \quad (22)$$

and \mathbf{F}_{k-1}^L and \mathbf{G}_{k-1}^L are formulated as follows, respectively.

$$\mathbf{F}_{k|k-1}^L = \begin{bmatrix} \mathbf{F}_i^L & \mathbf{F}_s^L \\ \mathbf{0}_{6 \times 9} & \mathbf{0}_{6 \times 6} \end{bmatrix}, \mathbf{G}_{k|k-1}^L = \begin{bmatrix} -\mathbf{I}_6 \\ \mathbf{0}_{9 \times 6} \end{bmatrix} \quad (23)$$

with

$$\mathbf{F}_i^L = \begin{bmatrix} -\tilde{\omega}_{ib}^b \times & \mathbf{0}_3 & \mathbf{0}_3 \\ -\tilde{\mathbf{f}}_{ib}^b \times & -\tilde{\omega}_{ib}^b \times & \mathbf{0}_3 \\ \mathbf{0}_3 & \mathbf{I}_3 & -\tilde{\omega}_{ib}^b \times \end{bmatrix}, \mathbf{F}_s^L = \begin{bmatrix} -\mathbf{I}_6 \\ \mathbf{0}_{3 \times 6} \end{bmatrix} \quad (24)$$

In addition, the left invariant error-based NHC measurement model is also better than right invariant error-based NHC measurement model, and its simplified measurement equation is formulated as follows [18].

$$\mathbf{z}_{nhc,k}^L = \mathbf{H}_{nhc}^L \mathbf{x}_{k|k-1}^L + \nu_{nhc} \quad (25)$$

where \mathbf{z}_{nhc}^L denotes the the difference variables between the measurement and estimated state, and ν_{nhc} denotes measurement noise. In addition, the simplified measurement matrix \mathbf{H}_{nhc}^L is formulated as follows

$$\mathbf{H}_{nhc}^L = \begin{bmatrix} \mathbf{h}_{\{1,1\}}^L & \mathbf{h}_{\{1,2\}}^L & \mathbf{0}_{1 \times 3} & \mathbf{0}_{1 \times 3} & \mathbf{0}_{1 \times 3} \\ \mathbf{h}_{\{2,1\}}^L & \mathbf{h}_{\{2,2\}}^L & \mathbf{0}_{1 \times 3} & \mathbf{0}_{1 \times 3} & \mathbf{0}_{1 \times 3} \end{bmatrix} \quad (26)$$

where

$$\begin{cases} \mathbf{h}_{\{1,1\}}^L = -\bar{\mathbf{C}}_b^u (\mathbf{v}_{sins}^b) \times (1,:) \\ \mathbf{h}_{\{1,2\}}^L = -\bar{\mathbf{C}}_b^u (1,:) \end{cases} \quad (27)$$

and

$$\begin{cases} \mathbf{h}_{\{2,1\}}^L = -\bar{\mathbf{C}}_b^u (\mathbf{v}_{sins}^b) \times (3,:) \\ \mathbf{h}_{\{2,2\}}^L = -\bar{\mathbf{C}}_b^u (3,:) \end{cases} \quad (28)$$

where $\bar{\mathbf{C}}_b^u$ denote the estimated mounting error angle matrix by the proposed method, whose initial value is set as \mathbf{I}_3 .

B. Proposed velocity-bias-based mounting error angle estimation method

1) NIW-based velocity bias estimation within the VB framework: Aiming at the problems of existing mounting error angle estimation methods, the velocity-bias-based mounting error angle estimation method is proposed. Compared with the existing direct method which uses the mounting error angle as the estimated state, the proposed method estimates the velocity bias vector induced by the mounting error angle, so it has the advantage of decoupling from the inaccurate navigation state. Based on the analysis in Section III, the PDF of noise ν_{nhc} can be assumed to follow a biased Gaussian distribution with an unknown bias vector \mathbf{u}_k and covariance \mathbf{R}_k , namely, $\nu_k \sim N(\mathbf{x}_k; \mathbf{u}_k, \mathbf{R}_k)$. Accordingly, to estimate \mathbf{u}_k , the NIW distribution is introduced as follows [43].

$$\begin{cases} p(\mathbf{x}|\mathbf{u}, \mathbf{R}) = N(\mathbf{x}; \mathbf{u}, \mathbf{R}) \\ p(\mathbf{u}, \mathbf{R}) = NIW(\mathbf{u}, \mathbf{R}; \mathbf{u}_0, \lambda, t, \mathbf{T}) \\ = N(\mathbf{u}; \mathbf{u}_0, \mathbf{R}/\lambda) IW(\mathbf{R}; t, \mathbf{T}) \end{cases} \quad (29)$$

where the \mathbf{u} and \mathbf{R} denote the non-zero mean and covariance matrix, respectively, and the \mathbf{u}_0 , λ , t , and \mathbf{T} denote the location parameter, the scale parameter, the degrees of freedom parameter, and the scale matrix, respectively. Then, joint PDF of \mathbf{u}_k and \mathbf{R}_k is modelled as follows [43].

$$\begin{aligned} p(\mathbf{u}_k, \mathbf{R}_k) &= NIW(\mathbf{u}_k, \mathbf{R}_k; \hat{\mathbf{u}}_{k|k-1}, \hat{\lambda}_{k|k-1}, \hat{t}_{k|k-1}, \hat{\mathbf{T}}_{k|k-1}) \\ &= N(\mathbf{u}_k; \hat{\mathbf{u}}_{k|k-1}, \mathbf{R}_k/\hat{\lambda}_{k|k-1}) \\ &\quad \times IW(\mathbf{R}_k; \hat{t}_{k|k-1}, \hat{\mathbf{T}}_{k|k-1}) \end{aligned} \quad (30)$$

where the $\hat{\mathbf{u}}_{k|k-1}$, $\hat{\lambda}_{k|k-1}$, $\hat{t}_{k|k-1}$, and $\hat{\mathbf{T}}_{k|k-1}$, are prior parameters, the parameters are calculated as follows [34].

$$\begin{cases} \hat{\mathbf{u}}_{k|k-1} = \hat{\mathbf{u}}_{k-1} & \hat{\lambda}_{k|k-1} = \rho \hat{\lambda}_{k-1} \\ \hat{t}_{k|k-1} = \rho \hat{t}_{k-1} & \hat{\mathbf{T}}_{k|k-1} = \rho \hat{\mathbf{T}}_{k-1} \end{cases} \quad (31)$$

where $\rho \in (0, 1]$ is a forgetting factor. The conditional likelihood PDF $p(\mathbf{z}_k|\mathbf{x}_k^L, \mathbf{u}_k, \mathbf{R}_k)$ can be naturally formulated as the Gaussian distribution, i.e.,

$$\begin{aligned} p(\mathbf{z}_k|\mathbf{x}_k^L, \mathbf{u}_k, \mathbf{R}_k) &= p_{\nu_k}(\mathbf{z}_k - \mathbf{H}_k^L \mathbf{x}_k^L) \\ &= N(\mathbf{z}_k; \mathbf{H}_k^L \mathbf{x}_k^L + \mathbf{u}_k, \mathbf{R}_k) \end{aligned} \quad (32)$$

In addition, the one-step prediction PDF $p(\mathbf{x}_k^L|\mathbf{z}_{1:k-1})$ is written as follows.

$$p(\mathbf{x}_k^L|\mathbf{z}_{1:k-1}) = N(\mathbf{x}_k^L; \hat{\mathbf{x}}_{k|k-1}^L, \mathbf{P}_{k|k-1}^L) \quad (33)$$

where $\hat{\mathbf{x}}_{k|k-1}^L$ and $\mathbf{P}_{k|k-1}^L$ are obtained as follows.

$$\begin{aligned} \hat{\mathbf{x}}_{k|k-1}^L &= \mathbf{F}_{k-1}^L \hat{\mathbf{x}}_{k-1|k-1}^L \\ \mathbf{P}_{k|k-1}^L &= \mathbf{F}_{k-1}^L \mathbf{P}_{k-1|k-1}^L (\mathbf{F}_{k-1}^L)^T + \mathbf{G}_{k-1}^L \mathbf{Q}_{k-1} (\mathbf{G}_{k-1}^L)^T \end{aligned} \quad (34)$$

In order to jointly estimate $\Xi \triangleq \{\mathbf{x}_k^L, \mathbf{u}_k, \mathbf{R}_k\}$, the VB method is introduced, which minimizes the Kullback-Leibler divergence (KLD) between the approximate and true joint posterior distributions via fixed-point iteration. Then, the approximate posterior PDF of Ξ satisfies as follow [34]

$$\log q(\vartheta) = E_{\Xi-\vartheta} [\log p(\Xi, \mathbf{z}_{1:k})] + c_\vartheta \quad (35)$$

where the variable ϑ denotes the elements of the set $\Xi \triangleq \{\mathbf{x}_k^L, \mathbf{u}_k, \mathbf{R}_k\}$, and $\Xi^{-\vartheta}$ denotes the variables of Ξ except for the variable ϑ , and c_ϑ denotes the constant about ϑ , and the joint PDF $p(\mathbf{x}_k^L, \mathbf{u}_k, \mathbf{R}_k, \mathbf{z}_{1:k})$ is given by

$$p(\Xi, \mathbf{z}_{1:k}) = p(\mathbf{z}_k | \mathbf{x}_k^L, \mathbf{u}_k, \mathbf{R}_k) p(\mathbf{x}_k^L | \mathbf{z}_{1:k-1}) p(\mathbf{u}_k, \mathbf{R}_k) \times p(\mathbf{z}_{1:k-1}) \quad (36)$$

and based on (30), (32), and (33), the $\log p(\Xi, \mathbf{z}_{1:k})$ can be formulated as follows.

$$\begin{aligned} \log p(\Xi, \mathbf{z}_{1:k}) &= -\frac{1}{2} \log |\mathbf{R}_k| - \frac{1}{2} (\mathbf{z}_k - \mathbf{H}_k^L \mathbf{x}_k^L - \mathbf{u}_k)^T \mathbf{R}_k^{-1} \\ &\times (\mathbf{z}_k - \mathbf{H}_k^L \mathbf{x}_k^L - \mathbf{u}_k) + \log N(\mathbf{x}_k^L; \hat{\mathbf{x}}_{k|k-1}^L, \mathbf{P}_{k|k-1}^L) \\ &- \frac{1}{2} \log |\mathbf{R}_k| - \frac{1}{2} \hat{\lambda}_{k|k-1} (\mathbf{u}_k - \hat{\mathbf{u}}_{k|k-1})^T \mathbf{R}_k^{-1} (\mathbf{u}_k - \hat{\mathbf{u}}_{k|k-1}) \\ &- \frac{1}{2} (\hat{t}_{k|k-1} + d + 1) \log |\mathbf{R}_k| - \frac{1}{2} \text{tr}(\hat{\mathbf{T}}_{k|k-1} \mathbf{R}_k^{-1}) + c_\Xi \end{aligned} \quad (37)$$

where d denotes the dimensions of measurement vector. Subsequently, let $\vartheta = \mathbf{x}_k^L$ and substitute (37) into (35), the approximate posterior PDF $q^{(i+1)}(\mathbf{x}_k^L)$ is given by

$$q^{(i+1)}(\mathbf{x}_k^L) = N(\mathbf{x}_k^L; \hat{\mathbf{x}}_{k|k}^{L,(i+1)}, \mathbf{P}_{k|k}^{L,(i+1)}) \quad (38)$$

where $\hat{\mathbf{x}}_{k|k}^{L,(i+1)}$ and $\mathbf{P}_{k|k}^{L,(i+1)}$ are, respectively, formulated as follows [43]

$$\begin{cases} \hat{\mathbf{R}}_k^{(i+1)} = \{E^{(i+1)}[\mathbf{R}_k^{-1}]\}^{-1} \\ \mathbf{K}_k^{(i+1)} = \mathbf{P}_{k|k-1}^L (\mathbf{H}_k^L)^T (\mathbf{H}_k^L \mathbf{P}_{k|k-1}^L (\mathbf{H}_k^L)^T + \hat{\mathbf{R}}_k^{(i+1)})^{-1} \\ \mathbf{x}_{k|k}^{L,(i+1)} = \hat{\mathbf{x}}_{k|k-1}^L + \mathbf{K}_k^{(i+1)} (\mathbf{z}_k - \mathbf{H}_k^L \hat{\mathbf{x}}_{k|k-1}^L - E^{(i+1)}[\mathbf{u}_k]) \\ \mathbf{P}_{k|k}^{L,(i+1)} = (\mathbf{I}_{15} - \mathbf{K}_k^{(i+1)} \mathbf{H}_k^L) \mathbf{P}_{k|k-1}^L \end{cases} \quad (39)$$

Additionally, let $\vartheta = \{\mathbf{u}_k, \mathbf{R}_k\}$ and substitute (37) into (35), the approximate posterior PDF $q^{(i+1)}(\mathbf{u}_k, \mathbf{R}_k)$ is given by

$$\begin{aligned} q^{(i+1)}(\mathbf{u}_k, \mathbf{R}_k) &= N(\mathbf{u}_k; \hat{\mathbf{u}}_{k|k}^{(i+1)}, \mathbf{R}_k / \hat{\lambda}_{k|k}^{(i+1)}) \\ &\times IW(\mathbf{R}_k; \hat{t}_{k|k}^{(i+1)}, \hat{\mathbf{T}}_{k|k}^{(i+1)}) \end{aligned} \quad (40)$$

where the updated parameters $\hat{\mathbf{u}}_{k|k}^{(i+1)}$, $\hat{\lambda}_{k|k}^{(i+1)}$, $\hat{t}_{k|k}^{(i+1)}$ and $\hat{\mathbf{T}}_{k|k}^{(i+1)}$ are, respectively, formulated as [43]

$$\begin{cases} \hat{\lambda}_{k|k}^{(i+1)} = \hat{\lambda}_{k|k-1} + 1 \\ \hat{\mathbf{u}}_{k|k}^{(i+1)} = (\hat{\lambda}_{k|k-1} \hat{\mathbf{u}}_{k|k-1} + \tilde{\mathbf{z}}_k^{(i+1)}) / \hat{\lambda}_{k|k}^{(i+1)} \\ \hat{t}_{k|k}^{(i+1)} = \hat{t}_{k|k-1} + 1 \\ \hat{\mathbf{T}}_{k|k}^{(i+1)} = \hat{\mathbf{T}}_{k|k-1} + \mathbf{H}_k^L \mathbf{P}_{k|k}^{L,(i+1)} (\mathbf{H}_k^L)^T \\ + \frac{\hat{\lambda}_{k|k-1}}{\hat{\lambda}_{k|k}^{(i+1)}} (\tilde{\mathbf{z}}_k^{(i+1)} - \hat{\mathbf{u}}_{k|k-1})(\tilde{\mathbf{z}}_k^{(i+1)} - \hat{\mathbf{u}}_{k|k-1})^T \end{cases} \quad (41)$$

where the parameter $\tilde{\mathbf{z}}_k^{(i+1)}$ is given by

$$\tilde{\mathbf{z}}_k^{(i+1)} = \mathbf{z}_k - \mathbf{H}_k^L \hat{\mathbf{x}}_{k|k}^{L,(i+1)} \quad (42)$$

and the expectations $E^{(i+1)}[\mathbf{u}_k]$ and $E^{(i+1)}[\mathbf{R}_k^{-1}]$ in (39) are, respectively, formulated as follows

$$\begin{cases} E^{(i+1)}[\mathbf{u}_k] = \hat{\mathbf{u}}_{k|k}^{(i+1)} \\ E^{(i+1)}[\mathbf{R}_k^{-1}] = \hat{t}_{k|k}^{(i+1)} (\hat{\mathbf{T}}_{k|k}^{(i+1)})^{-1} \end{cases} \quad (43)$$

2) *Calculate the mounting error angle through estimated velocity bias:* According to the analyses in Section III, the mounting error angle $[\alpha, \gamma]$ can be approximately calculated from the estimated velocity bias $\hat{\mathbf{u}}_{k|k}$. Then, using (6), it can be reformulated as follows

$$\begin{cases} \hat{\mathbf{u}}_{k|k}(1) \simeq \gamma v^u \\ \hat{\mathbf{u}}_{k|k}(2) \simeq \alpha v^u \end{cases} \quad (44)$$

where $\hat{\mathbf{u}}_{k|k}(1)$ and $\hat{\mathbf{u}}_{k|k}(2)$ denote the velocity biases induced by the mounting error angle, and v^u denotes the vehicle velocity, and the mounting error angle can be calculated as follows

$$\begin{cases} \hat{\gamma} \simeq (v^u)^{-1} \hat{\mathbf{u}}_{k|k}(1) \\ \hat{\alpha} \simeq (v^u)^{-1} \hat{\mathbf{u}}_{k|k}(2) \end{cases} \quad (45)$$

where $v^u = \sqrt{v_E^2 + v_N^2 + v_U^2}$, and v_E , v_N , and v_U denote the integrated navigation velocity in east, north, and up, respectively. Additionally, since the estimated mounting error angle $[\alpha, \gamma]$ are constant values, the higher the vehicle velocity, the greater the corresponding velocity bias $\hat{\mathbf{u}}_{k|k}$. As a result, the velocity bias is quickly estimated by (41). In addition, compared with the direct estimation method in [28], it can be found that the estimated velocity bias is more independent of the inaccurate state in the left invariant error-based SSM framework, so the estimation consistency of the velocity bias is better. This conclusion will be verified in Section VI and VII. Subsequently, in the following section V. A, the calculated mounting error angle further refine the NHC/OD submodels in (48) and (52), so as to further improve the consistency of the IMM estimation method. The pseudo-code of proposed method is shown in algorithm 1.

V. PROPOSED LIE GROUP-BASED RELIABLE IMM METHOD FOR SINS/GNSS/OD/NHC

A. Lie group consistent SSM-based IMM for SINS/GNSS/OD/NHC integrated navigation method

To enhance the estimation consistency, the Lie group-based SSM is proposed. It is well-known that the state independence of the left invariant error equation is better than that of the right invariant error equation, especially in the low-accuracy SINS. Accordingly, the left invariant error-based SSM is adopted in the proposed method, and it is reformulated as follows.

$$\mathbf{x}_{k|k-1}^L = \mathbf{F}_{k|k-1}^L \mathbf{x}_{k-1}^L + \mathbf{G}_{k-1}^L \mathbf{w}_b \quad (46)$$

where \mathbf{x}_{k-1}^L , $\mathbf{F}_{k|k-1}^L$, \mathbf{G}_{k-1}^L , and \mathbf{w}_b are defined in (21)-(24), and all subfilter state equations are based on (46). Additionally, for the NHC subfilter measurement equation, it is reformulated as follows [18].

$$[\mathbf{z}_{\text{nhc},k}^L]^{1-\text{th}} = [\mathbf{H}_{\text{nhc}}^L \mathbf{x}_{k|k-1}^L]^{1-\text{th}} + [\boldsymbol{\nu}_{\text{nhc}}]^{1-\text{th}} \quad (47)$$

Algorithm 1: The pseudo-code of the proposed velocity-bias-based estimation method.

Inputs: $\hat{\mathbf{x}}_{k|k-1}^L, \mathbf{P}_{k|k-1}^L, \mathbf{F}_k^L, \mathbf{G}_k^L, \mathbf{H}_k^L, \mathbf{z}_k, \tilde{\mathbf{Q}}_{k|k-1}, \mathbf{R}_k, \hat{\mathbf{u}}_{k|k-1}, \hat{\lambda}_{k|k-1}, \hat{t}_{k|k-1}, \hat{\mathbf{T}}_{k|k-1}, \rho, N_m$

Time update:

1. Calculate predicted state vector $\hat{\mathbf{x}}_{k|k-1}^L$ and $\mathbf{P}_{k|k-1}^L$

$$\hat{\mathbf{x}}_{k|k-1}^L = \mathbf{F}_k^L \hat{\mathbf{x}}_{k|k-1}^L$$

$$\mathbf{P}_{k|k-1}^L = \mathbf{F}_k^L \mathbf{P}_{k|k-1}^L (\mathbf{F}_k^L)^T + \mathbf{G}_k^L \mathbf{Q}_{k|k-1} (\mathbf{G}_k^L)^T$$

2. Calculate $\hat{\mathbf{u}}_{k|k-1}$, $\hat{\lambda}_{k|k-1}$, $\hat{t}_{k|k-1}$, and $\hat{\mathbf{T}}_{k|k-1}$:

$$\hat{\mathbf{u}}_{k|k-1} = \hat{\mathbf{u}}_{k|k-1}, \hat{\lambda}_{k|k-1} = \rho \hat{\lambda}_{k|k-1}$$

$$\hat{t}_{k|k-1} = \rho \hat{t}_{k|k-1}, \hat{\mathbf{T}}_{k|k-1} = \rho \hat{\mathbf{T}}_{k|k-1}$$

Iterated measurement update based on the proposed method:

3. Iterative Initialization:

$$\hat{\mathbf{x}}_{k|k}^{L,(0)} = \mathbf{x}_{k|k-1}^L, \mathbf{P}_{k|k}^{L,(0)} = \mathbf{P}_{k|k-1}^L, \hat{\mathbf{u}}_{k|k}^{(0)} = \hat{\mathbf{u}}_{k|k-1}$$

$$\mathbf{E}[\mathbf{R}_k^{(0)}]^{-1} = t_{k|k-1} (\mathbf{T}_{k|k-1})^{-1},$$

for $i = 0 : N_m - 1$

4. Update the estimated state $\hat{\mathbf{x}}_{k|k}^{L,(i+1)}$ and $\mathbf{P}_{k|k}^{L,(i+1)}$

$$\hat{\mathbf{R}}_k^{(i+1)} = \{\mathbf{E}^{(i+1)}[\mathbf{R}_k^{-1}]\}^{-1}$$

$$\mathbf{K}_{k|k}^{L,(i+1)} = \mathbf{P}_{k|k-1}^L (\mathbf{H}_k^L)^T (\mathbf{H}_k^L \mathbf{P}_{k|k-1}^L (\mathbf{H}_k^L)^T + \hat{\mathbf{R}}_k^{(i+1)})^{-1}$$

$$\mathbf{x}_{k|k}^{L,(i+1)} = \hat{\mathbf{x}}_{k|k-1}^L + \mathbf{K}_{k|k}^{L,(i+1)} (\mathbf{z}_k - \mathbf{H}_k^L \hat{\mathbf{x}}_{k|k-1}^L - \mathbf{E}^{(i+1)}[\mathbf{u}_k])$$

$$\mathbf{P}_{k|k}^{L,(i+1)} = (\mathbf{I}_{15} - \mathbf{K}_{k|k}^{L,(i+1)} \mathbf{H}_k^L) \mathbf{P}_{k|k-1}^L$$

5. Update the $\hat{\lambda}_{k|k}^{(i+1)}$, $\hat{\mathbf{u}}_{k|k}^{(i+1)}$, $\hat{t}_{k|k}^{(i+1)}$, $\hat{\mathbf{T}}_{k|k}^{(i+1)}$

$$\hat{\lambda}_{k|k}^{(i+1)} = \hat{\lambda}_{k|k-1} + 1$$

$$\hat{\mathbf{u}}_{k|k}^{(i+1)} = (\hat{\lambda}_{k|k-1} \hat{\mathbf{u}}_{k|k-1} + \tilde{\mathbf{z}}_k^{(i+1)}) / \hat{\lambda}_{k|k}^{(i+1)}$$

$$\hat{t}_{k|k}^{(i+1)} = \hat{t}_{k|k-1} + 1$$

$$\hat{\mathbf{T}}_{k|k}^{(i+1)} = \hat{\mathbf{T}}_{k|k-1} + \mathbf{H}_k^L \mathbf{P}_{k|k}^{L,(i+1)} (\mathbf{H}_k^L)^T$$

$$+ \frac{\hat{\lambda}_{k|k-1}}{\hat{\lambda}_{k|k}^{(i+1)}} (\tilde{\mathbf{z}}_k^{(i+1)} - \hat{\mathbf{u}}_{k|k-1}) (\tilde{\mathbf{z}}_k^{(i+1)} - \hat{\mathbf{u}}_{k|k-1})^T$$

where

$$\tilde{\mathbf{z}}_k^{(i+1)} = \mathbf{z}_k - \mathbf{H}_k^L \hat{\mathbf{x}}_{k|k}^{L,(i+1)}$$

6. Update the expectations $\mathbf{E}^{(i+1)}[\mathbf{u}_k]$ and $\mathbf{E}^{(i+1)}[\mathbf{R}_k^{-1}]$

$$\mathbf{E}^{(i+1)}[\mathbf{u}_k] = \hat{\mathbf{u}}_{k|k}^{(i+1)}$$

$$\mathbf{E}^{(i+1)}[\mathbf{R}_k^{-1}] = \hat{t}_{k|k}^{(i+1)} (\hat{\mathbf{T}}_{k|k}^{(i+1)})^{-1}$$

Posterior states updates:

$$10. \hat{\mathbf{x}}_{k|k}^L = \hat{\mathbf{x}}_{k|k}^{L,(N_m)}, \hat{\mathbf{P}}_{k|k}^L = \mathbf{P}_{k|k}^{L,(N_m)}, \hat{\mathbf{u}}_{k|k} = \hat{\mathbf{u}}_{k|k}^{(N_m)},$$

$$\hat{\lambda}_{k|k} = \hat{\lambda}_{k|k}^{(N_m)}, \hat{t}_{k|k} = \hat{t}_{k|k}^{(N_m)}, \hat{\mathbf{T}}_{k|k} = \hat{\mathbf{T}}_{k|k}^{(N_m)}.$$

Outputs: $\hat{\mathbf{x}}_{k|k}^L, \mathbf{P}_{k|k}^L, \hat{\mathbf{u}}_{k|k}, \hat{t}_{k|k}, \hat{\mathbf{T}}_{k|k}, \hat{\lambda}_{k|k}$

where $[.]^{1-th}$ denotes the 1-th measurement equation in IMM, and the measurement matrix $[\mathbf{H}_{\text{nhc}}^L]^{1-th}$ is formulated as follows

$$[\mathbf{H}_{\text{nhc}}^L]^{1-th} = \begin{bmatrix} \mathbf{h}_{\{1,1\}}^L & \mathbf{h}_{\{1,2\}}^L & \mathbf{0}_{1 \times 3} & \mathbf{0}_{1 \times 3} & \mathbf{0}_{1 \times 3} \\ \mathbf{h}_{\{2,1\}}^L & \mathbf{h}_{\{2,2\}}^L & \mathbf{0}_{1 \times 3} & \mathbf{0}_{1 \times 3} & \mathbf{0}_{1 \times 3} \end{bmatrix} \quad (48)$$

where

$$\begin{cases} \mathbf{h}_{\{1,1\}}^L = -\bar{\mathbf{C}}_b^u (\mathbf{v}_{\text{sins}}^b) \times (1,:) \\ \mathbf{h}_{\{2,1\}}^L = -\bar{\mathbf{C}}_b^u (1,:) \end{cases} \quad (49)$$

and

$$\begin{cases} \mathbf{h}_{\{2,1\}}^L = -\bar{\mathbf{C}}_b^u (\mathbf{v}_{\text{sins}}^b) \times (3,:) \\ \mathbf{h}_{\{2,2\}}^L = -\bar{\mathbf{C}}_b^u (3,:) \end{cases} \quad (50)$$

where $\bar{\mathbf{C}}_b^u$ denote the estimated mounting error angle matrix in Section IV, and $(1,:)$ denotes the 1-th row of the corresponding matrix, and likewise $(3,:)$. Similar with the NHC subfilter measurement equation, the OD subfilter measurement equation is formulated as follows.

$$[\mathbf{z}_{\text{od},k}^L]^{2-th} = [\mathbf{H}_{\text{od}}^L \mathbf{x}_{k|k-1}^L]^{2-th} + [\boldsymbol{\nu}_{\text{od}}]^{2-th} \quad (51)$$

where $[\mathbf{z}_{\text{od}}^L]^{2-th}$ and $[\boldsymbol{\nu}_{\text{od}}]^{2-th}$ denote the difference measurement variables and noise of the 2-th model, respectively. Correspondingly, the simplified measurement matrix $[\mathbf{H}_{\text{od}}^L]^{2-th}$ is given as follows [20].

$$[\mathbf{H}_{\text{od}}^L]^{2-th} = [-\bar{\mathbf{C}}_b^u (\mathbf{v}_{\text{sins}}^b \times) \quad -\bar{\mathbf{C}}_b^u \quad \mathbf{0}_3 \quad \mathbf{0}_3 \quad \mathbf{0}_3] \quad (52)$$

Furthermore, for the GNSS subfilter measurement equation, it is formulated as follows.

$$[\mathbf{z}_{\text{gnss},k}^L]^{3-th} = [\mathbf{H}_{\text{gnss}}^L \mathbf{x}_{k|k-1}^L]^{3-th} + [\boldsymbol{\nu}_{\text{gnss}}]^{3-th} \quad (53)$$

where $[\mathbf{z}_{\text{gnss}}^L]^{3-th}$ and $[\boldsymbol{\nu}_{\text{gnss}}]^{3-th}$ denote the difference measurement variables and noise of the 3-th model, respectively. Correspondingly, the measurement matrix $[\mathbf{H}_{\text{gnss}}^L]^{3-th}$ is formulated as follows [23].

$$[\mathbf{H}_{\text{gnss}}^L]^{3-th} = \begin{bmatrix} \mathbf{0}_3 & \mathbf{C}_b^n & \mathbf{0}_3 & \mathbf{0}_3 & \mathbf{0}_3 \\ \mathbf{0}_3 & \mathbf{0}_3 & \mathbf{C}_b^n & \mathbf{0}_3 & \mathbf{0}_3 \end{bmatrix} \quad (54)$$

Remark 1. Different definitions of group errors yield left-invariant and right-invariant errors. From the state model perspective, the left-invariant state model offers better state independence, resulting in superior estimation consistency. For GNSS and NHC, both the state and measurement models align better with the left-invariant error model [18], [23]. However, OD model is more consistent with the right-invariant error model [20]. In such cases of suboptimal matching, balancing state independence between the state and measurement models is key to improve estimation consistency. Since the time update frequency is higher than the measurement update frequency, the low-accuracy integrated navigation depends more on the independence of the state equation. Based on this, the proposed method is based on left-invariant error SSM.

B. Dynamic likelihood adaptive mechanism-based reliable model probability update method

Based on the proposed consistent Lie group SSM, an enhanced dynamic likelihood adaptive mechanism-based model probability update is proposed to address the filtering instability caused by complex environments. The implementation of the proposed method is divided into four steps: interactive input, LIEKF-based model filtering, dynamic likelihood adaptive mechanism-based model probability update, and estimation fusion, as shown in Fig. 6. The specific steps are as follows.

Step 1: Interactive input

In the interactive input, the model set is set to $\mathbf{M} = [m^1, m^2, m^3]$, with transitions between models governed by a Markov process. The transition probability matrix is denoted as $[\mathbf{p}^{ij}]_{3 \times 3}$, where \mathbf{p}^{ij} represents the Markov transition probability from model m^i to model m^j . This matrix satisfies the condition that the sum of each row equals 1, and it typically exhibits diagonal dominance, with values generally determined by prior information. Additionally, based on the probabilities of individual subfilter models and the Markov transition probability, the model mixing probability can be calculated as follows.

$$\mu_{k-1}^{ij} = \frac{\mathbf{p}^{ij} \mu_{k-1}^i}{\sum_{i=1}^3 \mathbf{p}^{ij} \mu_{k-1}^i} \quad (55)$$

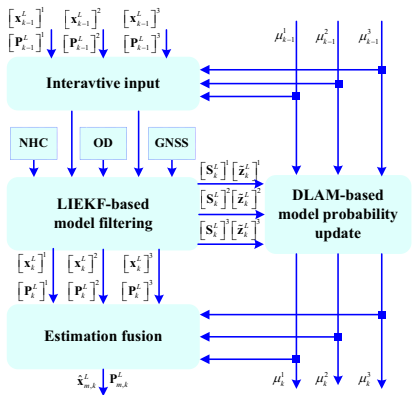


Fig. 6: The framework of proposed IMM estimation method.

where μ_{k-1}^{ij} denotes the model mixing probability from model m^i to model m^j at time $k-1$, and μ_{k-1}^i denotes the matching model probability of model m^i at time $k-1$. Additionally, the mixing state estimation $\hat{x}_{k-1}^{m,j}$ and its covariance matrix $\mathbf{P}_{k-1}^{m,j}$ can be calculated as follows.

$$\hat{x}_{k-1}^{m,j} = \sum_{i=1}^3 \hat{x}_{k-1}^{L,i} \mu_{k-1}^{ij} \quad (56)$$

$$\mathbf{P}_{k-1}^{m,j} = \sum_{i=1}^3 [\mathbf{P}_{k-1}^{L,i} + (\hat{x}_{k-1}^{L,i} - \hat{x}_{k-1}^{m,i})(\hat{x}_{k-1}^{L,i} - \hat{x}_{k-1}^{m,i})^T] \mu_{k-1}^{ij} \quad (57)$$

where $\hat{x}_{k-1}^{m,j}$ and $\mathbf{P}_{k-1}^{m,j}$ denote the mixing state estimation and its covariance matrix of model m^j at time $k-1$, respectively, and $\hat{x}_{k-1}^{L,i}$ and $\mathbf{P}_{k-1}^{L,i}$ denote the state estimation and its covariance matrix of model m^i at time $k-1$, respectively.

Step 2: LIEKF-based model filtering

Based on the mixing state vector $\hat{x}_{k-1}^{m,j}$ and its covariance matrix $\mathbf{P}_{k-1}^{m,j}$, the LIEKF-based filtering is performed individually. Accordingly, the state estimate and covariance matrix for each model at time k are obtained. For model m^j , the time update process is formulated as follows.

$$\hat{x}_{k|k-1}^{L,j} = \mathbf{F}_{k|k-1}^{L,j} \hat{x}_{k-1}^{m,j} \quad (58)$$

$$\mathbf{P}_{k|k-1}^{L,j} = \mathbf{F}_{k|k-1}^{L,j} \mathbf{P}_{k-1}^{m,j} \left(\mathbf{F}_{k|k-1}^{L,j} \right)^T + \mathbf{G}_{k-1}^{L,j} \mathbf{Q}_{k-1}^{j-1} \left(\mathbf{G}_{k-1}^{L,j} \right)^T \quad (59)$$

where $\mathbf{F}_{k|k-1}^{L,j} = \mathbf{F}_{k|k-1}^L$, $\mathbf{G}_{k-1}^{L,j} = \mathbf{G}_{k-1}^L$, $\mathbf{Q}_{k-1}^j = \mathbf{Q}_{k-1}$, and then the measurement innovation vector $\tilde{\mathbf{z}}_k^j$ and its covariance matrix \mathbf{S}_k^j are formulated as follows, respectively

$$\tilde{\mathbf{z}}_k^j = \mathbf{z}_k^{L,j} - \mathbf{H}_k^{L,j} \hat{x}_{k|k-1}^{L,j} \quad (60)$$

$$\mathbf{S}_k^j = \mathbf{H}_k^{L,j} \mathbf{P}_{k|k-1}^{L,j} \left(\mathbf{H}_k^{L,j} \right)^T + \mathbf{R}_k^j \quad (61)$$

where $\mathbf{z}_k^{L,j}$, $\mathbf{H}_k^{L,j}$, and \mathbf{R}_k^j are defined in Section V. A. Additionally, the associated parameters of $j=1$ to 3 correspond to NHC, OD, and GNSS, respectively. Then, the posterior state estimate $\hat{x}_k^{L,j}$ and its covariance matrix $\hat{\mathbf{P}}_k^{L,j}$ are formulated as follow, respectively

$$\hat{x}_k^{L,j} = \hat{x}_{k|k-1}^{L,j} + \mathbf{K}_k^j \tilde{\mathbf{z}}_k^j \quad (62)$$

$$\hat{\mathbf{P}}_k^{L,j} = \left(\mathbf{I}_{15} - \mathbf{K}_k^j \mathbf{H}_k^{L,j} \right) \mathbf{P}_{k|k-1}^{L,j} \quad (63)$$

and the Kalman gain \mathbf{K}_k^j is formulated as

$$\mathbf{K}_k^j = \mathbf{P}_{k|k-1}^{L,j} \left(\mathbf{H}_k^{L,j} \right)^T \left(\mathbf{S}_k^j \right)^{-1} \quad (64)$$

Step 3: Dynamic likelihood adaptive mechanism-based model probability update

Compared with existing methods, the proposed dynamic likelihood adaptive mechanism-based model probability update introduces the Gaussian likelihood function and the Student's t likelihood function as follows, respectively.

$$L_k^{G,j} = \frac{\exp \left(-\frac{1}{2} \left(\tilde{\mathbf{z}}_k^j \right)^T \left(\mathbf{S}_k^j \right)^{-1} \tilde{\mathbf{z}}_k^j \right)}{\sqrt{(2\pi)^d |\mathbf{S}_k^j|}} \quad (65)$$

and

$$L_k^{S,j} = \frac{\Gamma \left(\frac{\nu+d}{2} \right)}{\Gamma \left(\frac{\nu}{2} \right) \sqrt{(\nu\pi)^d |\mathbf{S}_k^j|}} \left(1 + \frac{\left(\tilde{\mathbf{z}}_k^j \right)^T \left(\mathbf{S}_k^j \right)^{-1} \tilde{\mathbf{z}}_k^j}{\nu} \right)^{-\frac{\nu+d}{2}} \quad (66)$$

where $L_k^{G,j}$ and $L_k^{S,j}$ denote the Gaussian likelihood value and the Student's t likelihood value of model m^j at time k , respectively, and d denotes the measurement dimension, and ν denotes the degrees of freedom parameter, and $\Gamma(\cdot)$ denotes the Gamma function. Subsequently, the Mahalanobis distance square of innovation vector and chi-square threshold are calculated, respectively. Furthermore, if the innovation vector is assumed to be the Gaussian distribution, the Mahalanobis distance square should follow the chi-square distribution, which is formulated as follows [46].

$$D^2 = \left(\tilde{\mathbf{z}}_k^j \right)^T \left(\mathbf{S}_k^j \right)^{-1} \tilde{\mathbf{z}}_k^j \sim \chi_d^2 \quad (67)$$

where D^2 denotes the Mahalanobis distance square, and χ_d^2 denotes the chi-square distribution. If the measurement noise is affected by the complex environments, the Mahalanobis distance square will exceed the chi-square distribution threshold. Correspondingly, the weight of the Student's t likelihood value is increased at a constant adjustment rate, and the weighted mixture likelihood value is obtained by combining it with the Gaussian likelihood value. The weighted mixture likelihood value is formulated as follows.

$$L_k^{m,j} = p_{\text{Gau}}^+ \cdot L_k^{G,j} + p_{\text{Stu}}^+ \cdot L_k^{S,j} \quad (68)$$

where

$$\begin{aligned} p_{\text{Gau}}^+ &= p_{\text{Gau}}^- (1 - \kappa) \\ p_{\text{Stu}}^+ &= 1 - p_{\text{Gau}}^+ \end{aligned} \quad (69)$$

where p_{Gau} and p_{Stu} denote the weights of Gaussian likelihood value and Student's t likelihood value, respectively, and $(\cdot)^-$ and $(\cdot)^+$ denote the prior and posterior values¹ respectively, and κ denotes the fixed adjustment rate. Otherwise, if

¹The p_{Gau}^- and p_{Stu}^- denote the prior weight value, and $0 \leq p_{\text{Gau}}^- \leq 1$, $0 \leq p_{\text{Stu}}^- \leq 1$, $p_{\text{Gau}}^- + p_{\text{Stu}}^- = 1$, and p_{Gau}^+ and p_{Stu}^+ are similar. Additionally, if the p_{Gau}^- is larger, the initial weight of Gaussian likelihood is larger. In this paper, $p_{\text{Gau}}^- = 0.8$, $p_{\text{Stu}}^- = 0.2$, which can effectively balance the accuracy and robustness.

the Mahalanobis distance square is less than the chi-square threshold, it is formulated as follows.

$$\begin{aligned} p_{\text{Gau}}^+ &= p_{\text{Gau}}^- (1 - \kappa) + \kappa \\ p_{\text{Stu}}^+ &= 1 - p_{\text{Gau}}^+ \end{aligned} \quad (70)$$

and the dynamic likelihood adaptive mechanism-based model probability update μ_k^j is formulated as follows.

$$\mu_k^j = \frac{L_k^{m,j} \sum_{i=1}^3 \mathbf{P}^{ij} \boldsymbol{\mu}_{k-1}^i}{\sum_{j=1}^3 \left(L_k^{m,j} \sum_{i=1}^3 \mathbf{P}^{ij} \boldsymbol{\mu}_{k-1}^i \right)} \quad (71)$$

Step 4: Estimation fusion

Finally, according to the subfilter estimates and the updated model probabilities, the weighted fusion is performed to obtain the fused state estimate $\hat{\mathbf{x}}_k^f$ and covariance matrix $\hat{\mathbf{P}}_k^f$, respectively, as shown below.

$$\hat{\mathbf{x}}_k^f = \sum_{j=1}^3 \hat{\mathbf{x}}_k^{L,j} \boldsymbol{\mu}_k^j \quad (72)$$

$$\hat{\mathbf{P}}_k^f = \sum_{j=1}^3 [\mathbf{P}_k^j + (\hat{\mathbf{x}}_k^{L,j} - \hat{\mathbf{x}}_k^f)(\hat{\mathbf{x}}_k^{L,j} - \hat{\mathbf{x}}_k^f)^T] \boldsymbol{\mu}_k^j \quad (73)$$

Furthermore, the modified navigation state estimate is formulated as follows.

$$\bar{\mathbf{x}}_k = \bar{\mathbf{x}}_k \exp \left(\hat{\mathbf{x}}_k^f (1 : 9) \right) \quad (74)$$

$$\hat{\mathbf{b}}_k = \bar{\mathbf{b}}_k + \hat{\mathbf{x}}_k^f (10 : 15) \quad (75)$$

where $\bar{\mathbf{x}}_k$ denotes the updated navigation states of SINS using (17), and similarly, $\bar{\mathbf{b}}_k$ denotes the updated inertial sensor bias using (19)-(20). The proposed Lie group-based reliable IMM method is composed of Section V. A-B, and the corresponding pseudo-code is shown in algorithm 2.

C. Estimation consistency analyses and discussions of the proposed method

To further demonstrate the theoretical advantages of the proposed method in estimation consistency, we will conduct qualitative analyses. Specifically, through the comparative analyses of the existing IMM-EKF method, the unique advantages of the core ideas behind the proposed method are revealed from the theoretical level. Based on the navigation state update equation in (17), the existing IMM-EKF state error variable is defined as follows [44]:

$$\mathbf{x}_{k-1} = [\phi^n \ \delta\mathbf{v} \ \delta\mathbf{r} \ \boldsymbol{\varepsilon}_b \ \boldsymbol{\nabla}_b]^T \quad (76)$$

where ϕ^n , $\delta\mathbf{v}$, and $\delta\mathbf{r}$ denote the corresponding the error of attitude, velocity, and position, respectively, and the subfilter state model is defined as follows:

$$\mathbf{F}_{k|k-1} = \begin{bmatrix} \mathbf{F}_i & \mathbf{F}_s \\ \mathbf{0}_{6 \times 9} & \mathbf{0}_{6 \times 6} \end{bmatrix}, \mathbf{G}_{k|k-1} = \begin{bmatrix} \mathbf{F}_s \\ \mathbf{0}_{9 \times 6} \end{bmatrix} \quad (77)$$

where the parameter matrices \mathbf{F}_i and \mathbf{F}_s are given by

$$\mathbf{F}_i = \begin{bmatrix} -\tilde{\omega}_{in}^n & \mathbf{0}_3 & \mathbf{0}_3 \\ (\tilde{\mathbf{C}}_b^n \tilde{\mathbf{C}}_b^b) \times & -\tilde{\omega}_{in}^n & \mathbf{0}_3 \\ \mathbf{0}_3 & \mathbf{I}_3 & -\tilde{\omega}_{in}^n \end{bmatrix}, \mathbf{F}_s = \begin{bmatrix} -\tilde{\mathbf{C}}_b^n & \mathbf{0}_3 \\ \mathbf{0}_3 & \tilde{\mathbf{C}}_b^n \end{bmatrix} \quad (78)$$

Algorithm 2: The Lie group-based reliable IMM estimation method for SINS/GNSS/OD/NHC integrated navigation.

Inputs: $\mathbf{x}_{k-1}^{L,j}$, $\mathbf{P}_{k-1}^{L,j}$, \mathbf{P}^{ij} , $\boldsymbol{\mu}_{k-1}^i$, $\mathbf{F}_{k|k-1}^{L,j}$, $\mathbf{G}_{k|k-1}^{L,j}$, \mathbf{Q}_{k-1}^j , \mathbf{R}_k^j , $\mathbf{z}_k^{L,j}$, $\mathbf{H}_k^{L,j}$, $\tilde{\mathbf{C}}_b^u$, $\hat{\mathbf{x}}_{k-1} = \{\mathbf{C}_b^n, \mathbf{v}_{ib}^n, \mathbf{r}_{ib}^n\}$, $\hat{\mathbf{b}}_{k-1} = \{\boldsymbol{\varepsilon}, \boldsymbol{\nabla}_b\}$, ν , d , $p_{\text{Gau}}^- = 0.8$, $p_{\text{Stu}}^- = 0.2$, κ , (where $i, j = 1$ to 3)

SINS state update:

1. Update the SINS state using (17).

Interactive input:

2. Calculate the model mixing probability $\boldsymbol{\mu}_{k-1}^{ij}$ using (55)

3. Calculate the mixing state estimate $\hat{\mathbf{x}}_{k-1}^{m,j}$ and corresponding covariance matrix $\mathbf{P}_{k-1}^{m,j}$ using (56) and (57), respectively.

LIEKF-based model filtering:

4. Calculate the one-step predicted state estimate $\hat{\mathbf{x}}_{k|k-1}^{L,j}$ of the subfilter and prediction error covariance matrix $\mathbf{P}_{k|k-1}^{L,j}$ using (58) and (59), respectively.

5. Calculate the measurement innovation vector $\tilde{\mathbf{z}}_k^j$ and innovation covariance matrix \mathbf{S}_k^j using (60) and (61), respectively.

6. Calculate the posterior state estimate $\hat{\mathbf{x}}_k^{L,j}$ and its covariance matrix $\hat{\mathbf{P}}_k^{L,j}$ using (62) and (63), respectively.

DLAM-based model probability update:

7. Calculate the Gaussian likelihood value $L_k^{G,j}$ and Student's t likelihood value $L_k^{S,j}$ using (65) and (66), respectively.

8. Determine Mahalanobis square distance and Chi-square threshold.

If $D^2 > \chi_d^2(\xi)$, then $p_{\text{Gau}}^+ = p_{\text{Gau}}^- (1 - \kappa)$, $p_{\text{Stu}}^+ = 1 - p_{\text{Gas}}^+$; else $p_{\text{Gau}}^+ = p_{\text{Gau}}^- (1 - \kappa) + \kappa$, $p_{\text{Stu}}^+ = 1 - p_{\text{Gau}}^+$, where d denotes the measurement dimension, and ξ denotes the significance level and $\xi = 0.05$.

9. Calculate the weighted mixture likelihood value $L_k^{m,j}$ using (68).

10. Calculate the DLAM-based model probability update $\boldsymbol{\mu}_k^j$ using (71).

Estimation fusion:

11. Calculate the fused state estimate $\hat{\mathbf{x}}_k^f$ and covariance matrix $\hat{\mathbf{P}}_k^f$ using (72) and (73), respectively.

12. Navigation state error correction using (74) and (75).

Outputs: $\hat{\mathbf{x}}_k$, $\hat{\mathbf{b}}_k$, $\boldsymbol{\mu}_k^j$, $\hat{\mathbf{x}}_k^{L,j}$, $\hat{\mathbf{P}}_k^{L,j}$, p_{Gas} , p_{Stu}^+ .

In addition, the corresponding traditional subfilter NHC measurement model is given as:

$$[\mathbf{H}_{\text{nhc}}]^{1-\text{th}} = \begin{bmatrix} \mathbf{h}_{\{1,1\}} & \mathbf{h}_{\{1,2\}} & \mathbf{0}_{1 \times 3} & \mathbf{0}_{1 \times 3} & \mathbf{0}_{1 \times 3} \\ \mathbf{h}_{\{2,1\}} & \mathbf{h}_{\{2,2\}} & \mathbf{0}_{1 \times 3} & \mathbf{0}_{1 \times 3} & \mathbf{0}_{1 \times 3} \end{bmatrix} \quad (79)$$

where

$$\begin{cases} \mathbf{h}_{\{1,1\}} = -\tilde{\mathbf{C}}_b^u \mathbf{C}_n^b (\mathbf{v}_{\text{sins}}^n) \times (1,:) \\ \mathbf{h}_{\{1,2\}} = \tilde{\mathbf{C}}_b^u \mathbf{C}_n^b (1,:) \end{cases} \quad (80)$$

$$\begin{cases} \mathbf{h}_{\{2,1\}} = -\tilde{\mathbf{C}}_b^u \mathbf{C}_n^b (\mathbf{v}_{\text{sins}}^n) \times (3,:) \\ \mathbf{h}_{\{2,2\}} = \tilde{\mathbf{C}}_b^u \mathbf{C}_n^b (1,:) \end{cases} \quad (81)$$

and the subfilter OD and GNSS measurement models are given as follow, respectively:

$$[\mathbf{H}_{\text{od}}]^{2-\text{th}} = [-\tilde{\mathbf{C}}_b^u \mathbf{C}_n^b (\mathbf{v}_{\text{sins}}^n) \times \tilde{\mathbf{C}}_b^u \mathbf{C}_n^b \ \mathbf{0}_3 \ \mathbf{0}_3 \ \mathbf{0}_3] \quad (82)$$

$$[\mathbf{H}_{\text{gnss}}]^{3-\text{th}} = [\mathbf{0}_{6 \times 3} \ \mathbf{I}_6 \ \mathbf{0}_{6 \times 3} \ \mathbf{0}_{6 \times 3}] \quad (83)$$

where the related states and parameters are defined in Section V. A, and (77)-(83) constitute the traditional subfilter SSM of the existing IMM-EKF method. Through comparative analyses, it can be seen that the accuracy of the subfiler state model (77) constructed based on traditional state error relies on inaccurate attitude matrix $\tilde{\mathbf{C}}_b^n$. Consequently, in the EKF-based IMM time update process similar to (58) and (59) in Section V. B, the attitude error matrix will affect the accuracy of the one-step prediction error covariance matrix through the state transition matrix. Meanwhile, the traditional subfilter

measurement models (79) and (82) are also susceptible to the inaccurate attitude matrix $\tilde{\mathbf{C}}_b^n$. Accordingly, in a similar subfilter measurement update (60)-(64), the inaccurate one-step prediction error covariance matrix and measurement model together cause the posterior estimate $\hat{\mathbf{x}}_k$ and the corresponding state error covariance matrix $\hat{\mathbf{P}}_{k|k}$ to decrease in accuracy. Subsequently, the posterior state error covariance matrix $\hat{\mathbf{P}}_{k|k}$ will further affect the prior accuracy of subfilter through interactive input (56) and (57). In contrast, from the perspective of model, the subfilter state model (23) and measurement models (48), (52) and (54) of the proposed method are more independent of the inaccurate attitude matrix $\tilde{\mathbf{C}}_b^n$, thus improving estimation consistency in the proposed LIEKF-based subfilter process. Although (54) appears to depend on the attitude matrix \mathbf{C}_b^n , it can be transformed into the innovation term that does not change the final estimation results [15].

Generally speaking, if the actual state error are consistent with the estimated state error covariance range, the filter is considered to have good estimation consistency, and the corresponding state error covariance matrix will gradually become stable. Meanwhile, the filter gain also tends to be stable, and the state estimation error gradually decreases to a finite range, thus achieving asymptotic convergence. To further analyze from a quantitative perspective, we use the normalized estimation error square (NEES) to evaluate consistency, which quantifies the relationship between the true estimation error and the theoretical prediction error, as defined below [17]:

$$\vartheta^i(t) \triangleq \frac{1}{d} \boldsymbol{\delta}^i(t)^T \mathbf{P}_c^i(t)^{-1} \boldsymbol{\delta}^i(t) \quad (84)$$

where d denotes the navigation state dimension, and $\boldsymbol{\delta}^i(t)$ denotes the estimated state error, and $\mathbf{P}_c^i(t)$ denotes the state estimation error covariance matrix. If the proposed method has better estimation consistency, $\vartheta^i(t)$ should fluctuate around 1, and the corresponding estimated error gradually decrease and converge. Conversely, if $\vartheta^i(t)$ deviates significantly from the theoretical value, it may indicate that the filter does not converge correctly. In Sections VI and VII, the corresponding consistency evaluation results of simulation and vehicle tests are given, respectively.

VI. SIMULATION TEST

In this section, the simulation is designed to verify the effectiveness of the proposed method in complex environments. The total time of the simulation trajectory is 500s. Correspondingly, the 150s-180s of the simulation trajectory is to estimate the mounting error angle, while the 180s-500s is set as complex navigation environments, as shown in Fig. 7. The GNSS measurement characteristics are generated as follows:

$$\left\{ \begin{array}{ll} \mathbf{v}_k \sim \begin{cases} N(\mathbf{0}, (\mathbf{r}_{gnss})^2) & \text{w.p. } p1 \\ N(\mathbf{0}, (15\mathbf{r}_{gnss})^2) & \text{w.p. } 1 - p1 \end{cases} & 300s \leq t_k < 350s \\ \mathbf{v}_k \sim N(\mathbf{0}, (\mathbf{r}_{gnss})^2) & \text{Other } t_k \end{array} \right. \quad (85)$$

where $\mathbf{r}_{gnss} = [0.1\text{m/s}; 1\text{m}]$, and w.p. denotes “with probability”, and $p1 = 0.95$ denotes the outlier probabilities. In

TABLE I: Inertial sensor parameters in the simulation.

Sensor	Constant drift	Random error
Gyroscope	50°/h	0.25°/√h
Accelerometer	2000ug	100ug/√Hz

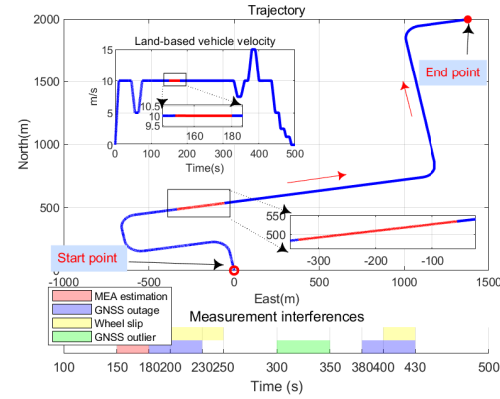


Fig. 7: The trajectory and interferences in the simulation.

addition, the odometer measurement characteristics are generated as follows:

$$\left\{ \begin{array}{ll} \mathbf{v}_k \sim \begin{cases} N(\mathbf{0}, (\mathbf{r}_{od})^2) & \text{w.p. } p2 \\ N(\mathbf{0}, (10\mathbf{r}_{od})^2) & \text{w.p. } 1 - p2 \end{cases} & 200s \leq t_k \leq 250s \\ \mathbf{v}_k \sim \begin{cases} N(\mathbf{0}, (\mathbf{r}_{od})^2) & \text{w.p. } p3 \\ N(\mathbf{0}, (15\mathbf{r}_{od})^2) & \text{w.p. } 1 - p3 \end{cases} & 400s \leq t_k \leq 430s \\ \mathbf{v}_k \sim N(\mathbf{0}, (\mathbf{r}_{od})^2) & \text{Other } t_k \end{array} \right. \quad (86)$$

where $\mathbf{r}_{od} = [0.1\text{m/s}]$, and $p2 = 0.90$ and $p3 = 0.95$. In simulation, the inertial sensor parameters are listed in Table I. In addition, the random errors of GNSS are set as 0.1m/s and 1m, and the random error of odometer is set as 0.1m/s. The output frequency of IMU is set as 100Hz, and GNSS and odometer are both set as 10Hz. The initial error of velocity and position are set as 0.1m/s and 1m, respectively, and the initial error of pitch, roll, heading are set as 15°, 15°, and 30°, respectively. To evaluate the estimation methods, the root-mean-square errors (RMSEs) is employed as performance metrics, and the RMSE is defined as follows.

$$\left\{ \text{RMSE}_{\hat{\mathbf{x}}_k} \triangleq \sqrt{\frac{1}{N_{MC}} \sum_{s=1}^{N_{MC}} (\mathbf{x}_k^s - \hat{\mathbf{x}}_k^s)^2} \right. \quad (87)$$

where \mathbf{x}_k^s and $\hat{\mathbf{x}}_k^s$ denote the true and estimated navigation state vectors at time k in the s -th Monte Carlo runs, respectively, and N_{MC} denotes the total Monte Carlo runs number.

A. Comparisons and analyses of proposed velocity-bias-based mounting error angle estimation method

In the simulation, the trajectory is set as in Fig. 7, the mounting error angle is estimated during 150s-180s when the vehicle maintain a constant speed of 10m/s. In addition,

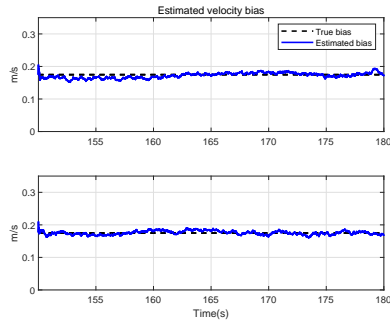


Fig. 8: The estimated velocity bias in the simulation.

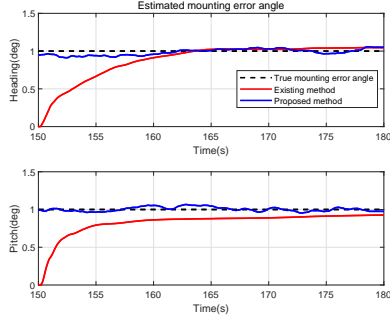


Fig. 9: The estimated mounting error angle in the simulation.

the initial value is set as $[\alpha, \gamma] = [1^\circ, 1^\circ]$. As a contrast method, the initial state of the existing EKF-based VDR is set as $\mathbf{x}_{vdr} = \mathbf{0}_{8 \times 1}$, and the state error covariance matrix \mathbf{P}_{vdr} is set as $\text{diag}([0.1\mathbf{I}_{3 \times 1}; 0.1^\circ \mathbf{I}_{2 \times 1}; 0.1^\circ \mathbf{I}_{3 \times 1}])^2$. The measurement noise covariance matrix $\mathbf{R}_{ma,k}$ and state noise covariance matrix $\mathbf{Q}_{ma,k}$ are set as $\text{diag}([0.1\mathbf{I}_{3 \times 1}])^2$ and $\text{diag}([0.01^\circ / \sqrt{h} \mathbf{I}_{3 \times 1}; 0.01^\circ / \sqrt{h} \mathbf{I}_{2 \times 1}])^2$. For the proposed velocity-bias-based mounting error angle estimation method in this paper, the initial state value is set as $\mathbf{x}_{mea} = \mathbf{0}_{15 \times 1}$, and the initial state error covariance matrix \mathbf{P}_{mea} is set as $\text{diag}([5^\circ \mathbf{I}_{3 \times 1}; 0.1m/\mathbf{I}_{3 \times 1}; 1m\mathbf{I}_{3 \times 1}; 5^\circ / h \mathbf{I}_{3 \times 1}; 200ug\mathbf{I}_{3 \times 1}])^2$, and NHC measurement noise covariance matrix \mathbf{R}_{nhc} and state noise covariance matrix \mathbf{Q}_k are set as $\text{diag}([0.05m/\mathbf{I}_{2 \times 1}])^2$ and $\text{diag}([0.15^\circ / \sqrt{h} \mathbf{I}_{3 \times 1}; 100ug / \sqrt{Hz} \mathbf{I}_{3 \times 1}])^2$, and $\hat{\mathbf{u}}_{k-1} = \mathbf{0}_2$, $\hat{\lambda}_{k-1} = 3 \cdot 10^{-3}$, $\hat{t}_{k-1} = 3$, $\hat{\mathbf{T}}_{k-1} = \hat{t}_{k-1} \mathbf{R}_{nhc}$, and $\rho = 1 - \exp(-6)$.

According to the set mounting error angle $[\alpha, \gamma] = [1^\circ, 1^\circ]$ and constant vehicle velocity 10m/s, the velocity bias can be calculated as follows.

$$\mathbf{u}_{bias} \simeq \begin{cases} \gamma v_y^u & = \begin{cases} 0.175 \text{ (m/s)} \\ 0.175 \text{ (m/s)} \end{cases} \end{cases} \quad (88)$$

As shown in the Fig. 8, the proposed velocity-bias-based mounting error angle estimation method can effectively and rapidly estimates the velocity bias vector. Specifically, when the vehicle maintains a constant speed, the mounting error angle introduces a velocity bias on axes perpendicular to the forward direction. Furthermore, as shown in the Fig. 9, the mounting error angle can be quickly calculated by (88). Although existing method can eventually converge to accurate values over time, the convergence time is significantly longer. Subsequently, the estimated mounting error angles are

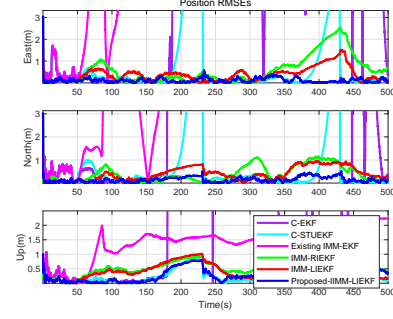


Fig. 10: The position RMSEs in the simulation.

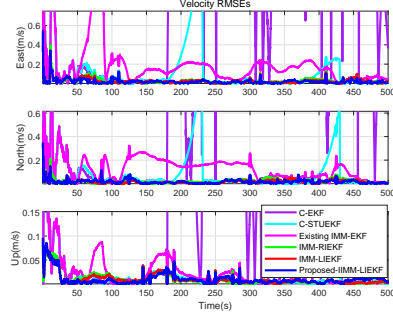


Fig. 11: The velocity RMSEs in the simulation.

compensated into the proposed Lie group-based reliable IMM algorithm to fully exploit the potential of OD/NHC.

B. Comparisons and analyses of the proposed reliable IMM method in complex environments

In this paper, the proposed method is specifically referred to as the improved IMM-based LIEKF (IIMM-LIEKF). To conduct the ablation simulation experiments, multiple comparison methods are selected with identical conditions. Firstly, the existing IMM-EKF method is compared with centralized EKF (C-EKF) and robust centralized Student's *t*-EKF (C-STUEKF) to verify the superiority of the IMM method in complex environments. Next, the IMM-LIEKF is compared with the existing IMM-EKF and IMM-RIEKF to evaluate the effectiveness of the left-invariant error-based consistent SSM. Finally, to verify the reliability of the proposed DLAM, the proposed IIMM-LIEKF is compared with the IMM-LIEKF. Subsequently, the advantages of the proposed IIMM-LIEKF are comprehensively validated through the comparisons of convergence accuracy and estimation consistency.

For the centralized methods, the initial setting of state error variable \mathbf{x}_{nav} , state noise covariance matrix \mathbf{Q}_k , and initial state error covariance matrix \mathbf{P}_0 are same as in Section VI. A. Additionally, the MNCM of OD \mathbf{R}_{od} , GNSS \mathbf{R}_{gnss} , and NHC \mathbf{R}_{nhc} , are set as $\text{diag}([0.05; 0.1; 0.05] \text{m/s})^2$, $\text{diag}([0.1m/\mathbf{I}_{3 \times 1}; 1m\mathbf{I}_{3 \times 1}])^2$, and $\text{diag}([0.05m/\mathbf{I}_{2 \times 1}])^2$, respectively, and the measurement noise covariance matrix \mathbf{R}_{cen} is set as $\text{blkdiag}([\mathbf{R}_{nhc}; \mathbf{R}_{od}; \mathbf{R}_{gnss}])$. Meanwhile, \mathbf{P}_0^R and \mathbf{P}_0^L of RIEKF and LIEKF are, respectively, formulated as

$$\mathbf{P}_0^R = \mathbf{N}_R \mathbf{P}_0 \mathbf{N}_R^T \quad (89)$$

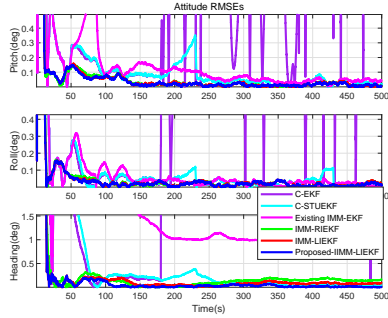


Fig. 12: The attitude RMSEs in the simulation.

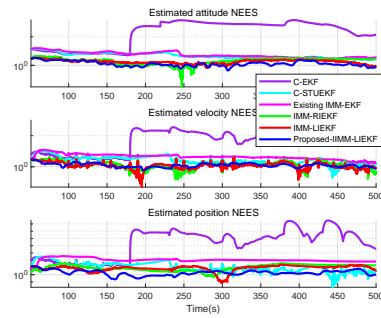


Fig. 14: NEES of navigation states in the simulation.

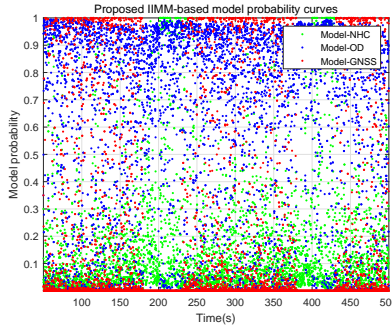


Fig. 13: The model probability curves in the simulation.

where

$$\mathbf{N}_R = \begin{bmatrix} \mathbf{I}_3 & \mathbf{0}_3 & \mathbf{0}_3 & \mathbf{0}_3 & \mathbf{0}_3 \\ (\mathbf{v}_{ib}^n) \times & -\mathbf{I}_3 & (\mathbf{C}_{e0}^{n0} \boldsymbol{\omega}_{ie}) \times & \mathbf{0}_3 & \mathbf{0}_3 \\ (\mathbf{r}_{ib}^n) \times & \mathbf{0}_3 & -\mathbf{I}_3 & \mathbf{0}_3 & \mathbf{0}_3 \\ \mathbf{0}_3 & \mathbf{0}_3 & \mathbf{0}_3 & \mathbf{I}_3 & \mathbf{0}_3 \\ \mathbf{0}_3 & \mathbf{0}_3 & \mathbf{0}_3 & \mathbf{0}_3 & \mathbf{I}_3 \end{bmatrix} \quad (90)$$

and

$$\mathbf{P}_0^L = \mathbf{N}_L \mathbf{P}_0 \mathbf{N}_L^T \quad (91)$$

where

$$\mathbf{N}_L = \begin{bmatrix} \mathbf{I}_3 & \mathbf{0}_3 & \mathbf{0}_3 & \mathbf{0}_3 & \mathbf{0}_3 \\ \mathbf{0}_3 & -\mathbf{C}_{n0}^{b0} & -\mathbf{C}_{n0}^{b0} (\mathbf{C}_{e0}^{n0} \boldsymbol{\omega}_{ie}) \times & \mathbf{0}_3 & \mathbf{0}_3 \\ \mathbf{0}_3 & \mathbf{0}_3 & -\mathbf{C}_{n0}^{b0} & \mathbf{0}_3 & \mathbf{0}_3 \\ \mathbf{0}_3 & \mathbf{0}_3 & \mathbf{0}_3 & \mathbf{I}_3 & \mathbf{0}_3 \\ \mathbf{0}_3 & \mathbf{0}_3 & \mathbf{0}_3 & \mathbf{0}_3 & \mathbf{I}_3 \end{bmatrix} \quad (92)$$

For the all IMM-based method, the initial model probabilities \mathbf{m}_{imm} are set as $[0.35; 0.35; 0.3]$, and the model probability transition matrix \mathbf{p}^{ij} is set as follow

$$\mathbf{p}^{ij} = \begin{bmatrix} 0.8 & 0.1 & 0.1 \\ 0.1 & 0.8 & 0.1 \\ 0.1 & 0.1 & 0.8 \end{bmatrix} \quad (93)$$

and the other initial parameters of IMM-subfilter 1-3 are set according to the preceding parameters. Additionally, for the proposed dynamic likelihood adaptive mechanism-based model probability update method, $p_{Gau}^- = 0.8$, $p_{Stu}^- = 0.2$, and the adaptive rate κ is set 0.1.

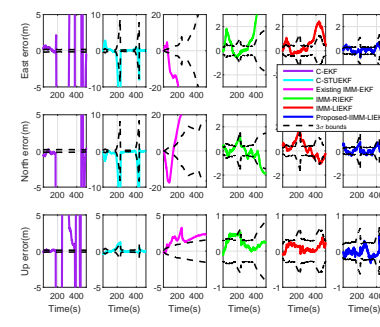


Fig. 15: 3σ bounds of the position error in the simulation.

1) Convergence accuracy comparisons and analyses: The RMSEs for position, velocity, and attitude are shown in Fig. 10-Fig. 12, respectively. The results indicate that the estimation accuracy of the C-EKF and C-STUEKF is relatively poor in complex environment. In contrast, the existing IMM-EKF method performs slightly better than both the C-EKF and C-STUEKF, demonstrating the superiority of the IMM estimation method in complex environments. Furthermore, the IMM-LIEKF outperforms the existing IMM-EKF and IMM-RIEKF, mainly due to the state independence provided by the left-invariant error-based consistent SSM, which ensures better estimation consistency. Based on this estimation consistency, the proposed IIMM-LIEKF incorporates the proposed DLAM to further improve the existing model probability update, effectively mitigating the negative impact of frequent model switching on estimation stability. Additionally, the model probability curves shown in Fig. 13 also illustrate the dynamic adaptability of the proposed IIMM-LIEKF. For example, during the GNSS outage from 180s to 230s, the OD model dominates due to its high measurement accuracy. Subsequently, when GNSS outage coincides with wheel slip within 200s to 230s, the NHC model probability increases. Finally, during the 230s-250s, when wheel slip occurs, the GNSS model probability once again becomes dominant.

2) Estimation consistency evaluations: To evaluate the estimation consistency, the corresponding NEES values are calculated for all methods. Fig. 14 shows the NEES of the estimated navigation states, which shows that the $\vartheta^i(t)$ of the proposed IIMM-LIEKF almost fluctuates around 1. Consequently, the proposed IIMM-LIEKF has better estimation consistency than other existing methods. The main reason is

TABLE II: Single-step execution times of comparison methods.

METHOD	C-EKF/STUEKF	IMM-EKF/RIEKF/LIEKF	Proposed IIMM-LIEKF [○]	Proposed IIMM-LIEKF [●]
TIME(ms)	4.25/5.65	14.31/14.51/14.55	23.85	15.88

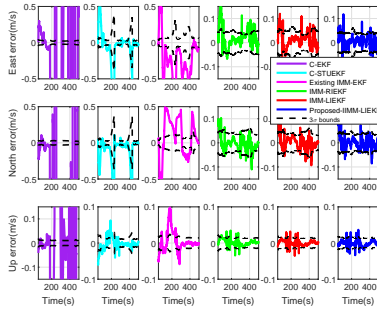


Fig. 16: 3σ bounds of the velocity error in the simulation.

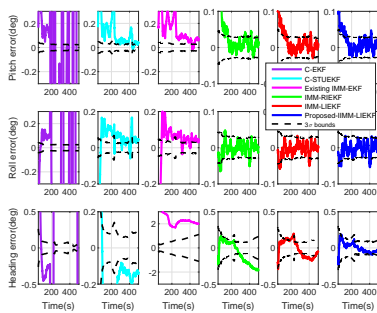


Fig. 17: 3σ bounds of the attitude error in the simulation.

that the proposed IIMM-LIEKF adopts a consistent Lie group framework, and the improvement of DLAM, which makes it have better consistency performance in complex environments. Additionally, the better the estimation consistency is, the higher the convergence accuracy can be obtained. To further analyze its convergence, the 3σ criterion is introduced, which has been widely used to evaluate the consistency performance of navigation estimation due to its applicability in a single simulation or experiment [13]. Specifically, the probability of $[\mu - 3\sigma, \mu + 3\sigma]$ is 0.9973, where μ is the mean value and σ is the standard deviation. Fig. 17 show the estimated navigation state errors and the corresponding 3σ bounds. The results indicate that the state estimation errors of the proposed method generally remain within the 3σ bounds. Additionally, the 3σ bounds of the proposed method change with the environment, which indicates that it has good adaptability and convergence to the uncertainty of the complex environment. In contrast, the estimation errors of other existing methods do not always stay within the 3σ bounds.

C. Computational demands comparison

To conveniently analyze the computational complex (CC) of the proposed method, we give the total floating-point operation of the existing IMM-EKF and the proposed IIMM-LIEKF based on algorithm 1-2. Actually, the proposed method

includes the mounting error angle estimation process and the reliable IMM-based integrated navigation process. Once the constant mounting error angle is accurately estimated, it is unnecessary to continue the mounting error angle estimation in the whole algorithm process; instead, only reliable IMM-based integrated navigation process needs to be executed. The corresponding floating-point operations are as follows:

$$\begin{aligned} CC_{IMM-EKF} = & 9n^3 + 27n^2 + 114n + 2m_a n + 3m_a n^2 \\ & + 2m_b n + 3m_a n^2 + 2m_b n + O(m_c^3) + 162 \end{aligned} \quad (94)$$

$$\begin{aligned} CC_{MEA} = & [3O(m_{nhc}) + 4m_{nhc}n^2 + 3m_{nhc}^2n + 3m_{nhc}^2 \\ & + 3m_{nhc}n + n^3 + 2m_{nhc} + 1] + O(m_{nhc}^3) + m_{nhc}^2 \\ & + 7n^2 + 2n^3 + 36n + 2m_{nhc} + 2 \end{aligned} \quad (95)$$

$$\begin{aligned} CC_{IIMM-LIEKF^\circ} = & 9n^3 + 27n^2 + 114n + 2m_a n + 3m_a n^2 \\ & + 2m_b n + 8O(m_c^3) + 6m_a + 4m_b \\ & + O(m_a/2) + 6O(3/2) + 169 \end{aligned} \quad (96)$$

$$CC_{IIMM-LIEKF^\bullet} = CC_{IIMM-LIEKF^\circ} + CC_{MEA} \quad (97)$$

and

$$\begin{aligned} m_a &= m_{nhc} + m_{gnss} + m_{od} \\ m_b &= m_{nhc}^2 + m_{gnss}^2 + m_{od}^2 \\ O(m_c^3) &= O(m_{nhc}^3 + m_{gnss}^3 + m_{od}^3) \end{aligned} \quad (98)$$

where $CC_{IMM-EKF}$, CC_{MEA} , $CC_{IIMM-LIEKF^\circ}$, and $CC_{IIMM-LIEKF^\bullet}$ denote the computational complexity of the existing method, the proposed mounting error angle estimation method, and the proposed IIMM-LIEKF (excluding the mounting error angle estimation), and the proposed IIMM-LIEKF (including the mounting error angle estimation), and m_{nhc} , m_{gnss} , m_{od} denote the measurement dimensions of NHC, GNSS, OD, respectively. Additionally, we also calculate the single-step execution time of each algorithm using Python performance profiling tools. The hardware environment is Intel Core i7-8750H processor at 2.20GHz. TABLE. II exhibits the single-step execution time. Through comparative analyses, the proposed IIMM-LIEKF[●] has slightly higher computational complexity compared to the other methods. After the mounting error angle estimation is completed, the computational complexity of the proposed IIMM-LIEKF[○] is comparable to those of existing IMM estimation methods.

VII. LAND VEHICLE FIELD TEST

In this section, the land vehicle field test is implemented to further verify the effectiveness of the proposed Lie group-based reliable IMM method, specially the proposed IIMM-LIEKF method. Since the primary objective is to verify the navigation method effectiveness for SINS/GNSS/OD/NHC in

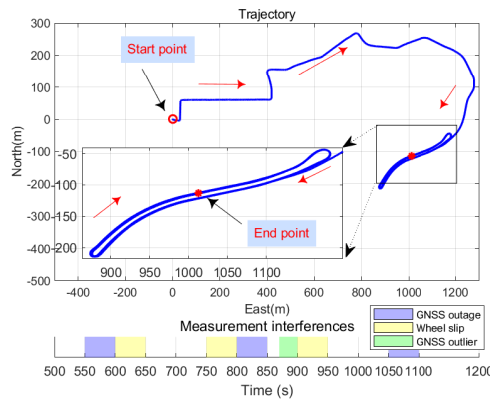


Fig. 18: The trajectory and interferences in the field test.

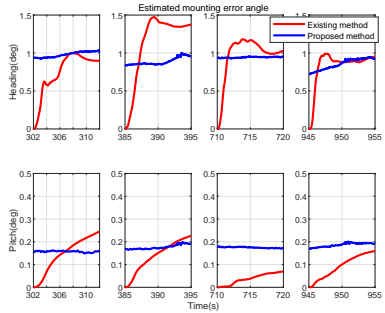


Fig. 19: The estimated mounting error angles in the field test.

complex navigation environments, we use a human-driven vehicle to conduct field test, and the on-board data are derived from the part of open source data [47]. The trajectory and added measurement interferences of land vehicle field test are shown in Fig. 18, and the total time is about 1200s. The platform of the land vehicle is composed of MEMS-IMU, GNSS, and odometer. The gyroscope bias and angle random walk are about $200^\circ/\text{h}$ and $0.24^\circ/\sqrt{\text{h}}$, respectively, and the accelerometer bias and velocity random walk are about $0.01\text{m}/\text{s}^2$ and $3\text{m}/\text{s}/\sqrt{\text{h}}$, respectively. Since the dataset only includes integrated SINS/GNSS data, we extracted the GNSS velocity and position data from it and added random noise of $0.1\text{m}/\text{s}$ and 1m , respectively. The output frequency of MEMS-IMU is 200Hz, and GNSS and odometer are both 2Hz. To further highlight the reliability of the proposed method in complex environments, we also introduce additional measurement faults into the original dataset as shown in Fig. 18. Additionally, the setting of GNSS outlier and wheel slip are similarly with (85) and (86), respectively.

1) Comparisons and analyses of proposed velocity-bias-based mounting error angle estimation method: For the existing EKF-based VDR method [28], the initial parameter settings are identical to those in Section VI. A, except for \mathbf{P}_{vdr} and $\mathbf{Q}_{\text{ma},k}$. In this part, \mathbf{P}_{vdr} and $\mathbf{Q}_{\text{ma},k}$ are set to $\text{diag}([1\mathbf{I}_{3 \times 1}; 0.25^\circ \mathbf{I}_{2 \times 1}; [0.1^\circ; 0.1^\circ; 0.5^\circ]]^2)$ and $\text{diag}([\frac{1}{10}^\circ / \sqrt{\text{h}} \mathbf{I}_{3 \times 1}; \frac{1}{10}^\circ / \sqrt{\text{h}} \mathbf{I}_{2 \times 1}]^2)$, respectively. In addition, for the proposed velocity-bias-based estimation method, the initial parameter settings are identical to those in Section VI.

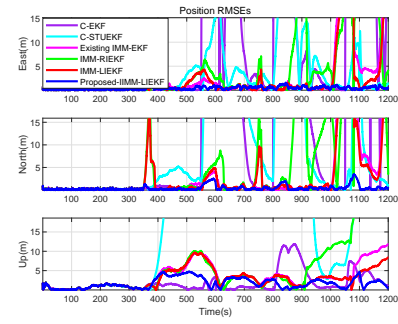


Fig. 20: The position RMSEs in the field test.

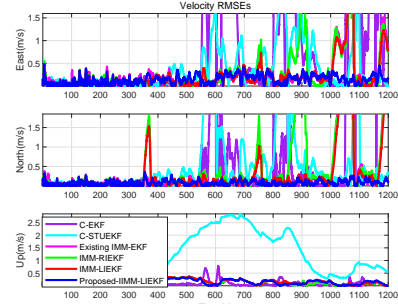


Fig. 21: The velocity RMSEs in the field test.

A, except for \mathbf{P}_{mea} and \mathbf{Q}_k . In this part, \mathbf{P}_{mea} and \mathbf{Q}_k are set to $\text{diag}([10^\circ \mathbf{I}_{3 \times 1}; \frac{1}{10} \text{m}/\text{s} \mathbf{I}_{3 \times 1}; 1\text{m} \mathbf{I}_{3 \times 1}; 90^\circ / \text{h} \mathbf{I}_{3 \times 1}; 2\text{mg} \mathbf{I}_{3 \times 1}]^2)$, and $\text{diag}([0.15^\circ / \sqrt{\text{h}} \mathbf{I}_{3 \times 1}; 300\text{ug} / \sqrt{\text{Hz}} \mathbf{I}_{3 \times 1}]^2)$. In the 1200s of the land-based vehicle field test, the constant velocity intervals at 302s-312s, 385s-395s, 710s-720s, and 945s-955s, are used to estimate the mounting error angle, respectively. As shown in the Fig. 19, the mounting error angle can be effectively calculated by the proposed velocity-bias-based estimation method. Although the true mounting error angle is unknown, the estimates in the proposed method is more consistent in different time intervals compared to the existing EKF-based VDR method.

2) Navigation state estimation in complex environments: Based on the estimated mounting error angle, the optimal framework of OD/NHC model is guaranteed, and then the effectiveness of the proposed Lie group-based reliable IMM integrated method is further validated. For the centralized method, the initial parameters of \mathbf{x}_{nav} , \mathbf{Q}_k , and \mathbf{P}_0 , are set as $\mathbf{0}_{15 \times 1}$, $\text{diag}([0.25^\circ / \sqrt{\text{h}} \mathbf{I}_{3 \times 1}; 100\text{ug} / \sqrt{\text{Hz}} \mathbf{I}_{3 \times 1}]^2)$, and $\text{diag}([5^\circ \mathbf{I}_{3 \times 1}; \frac{1}{10} \text{m}/\text{s} \mathbf{I}_{3 \times 1}; 1\text{m} \mathbf{I}_{3 \times 1}; 100^\circ / \text{h} \mathbf{I}_{3 \times 1}; \frac{1}{2} \text{mg} \mathbf{I}_{3 \times 1}]^2)$, respectively. Meanwhile, the setting of \mathbf{R}_{nhc} , \mathbf{R}_{od} , \mathbf{R}_{gnss} , and \mathbf{R}_{cen} are same with in Section VI. B. Similarly, the \mathbf{P}_0^R and \mathbf{P}_0^L of RIEKF and LIEKF should be also transformed by (89) and (91). Additionally, for the IMM-RIEKF, IMM-LIEKF, and proposed IMMI-LIEKF method, the setting of initial parameters are same with in the Section VI. B.

Fig. 20–Fig. 22 show the RMSEs of estimated navigation states. The estimated RMSEs results indicate that the C-EKF method and C-STUEKF method exhibit poor estimation accuracy, and IMM-based methods are generally better than C-EKF and C-STUEKF. For the IMM-based methods, the

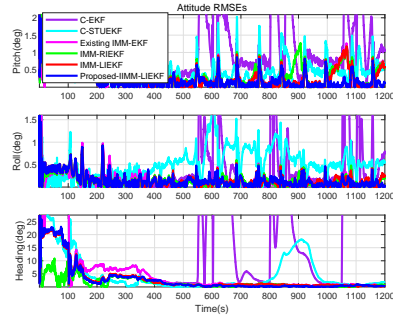


Fig. 22: The attitude RMSEs in the field test.

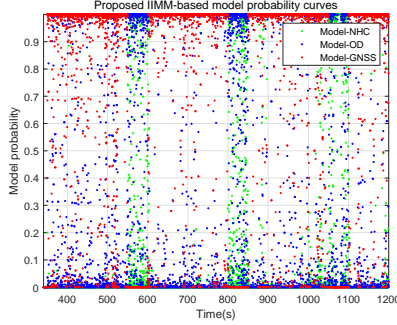


Fig. 23: The model probability curves in the field test.

IMM-LIEKF is slightly better than IMM-RIEKF, and far better than IMM-EKF. In addition, compared with other methods, the proposed IIMM-LIEKF method shows better reliability and estimation accuracy, especially in complex navigation environments with additional settings. The model probability curves in Fig. 23 reflect the current confidence of each submodel, and the curves changes also reflect the real-time adaptation of IMM method to dynamic environments. For instance, during the artificially set GNSS outages (550s-600s, 800s-850s, and 1050s-1100s), the probability of the GNSS model significantly approaches zero. Instead, the probability of the NHC and OD models increase, with the OD model exhibiting higher probability than NHC model. Fig. 24-Fig. 26 show the 3σ bounds of position error, velocity error, and attitude error, respectively. As compared to existing methods, the navigation errors of the proposed IIMM-LIEKF method are mostly contained within the 3σ bounds. Therefore, the land vehicle test results are in good agreement with the simulation results, which verifies the effective consistency of the proposed method in real scenarios.

VIII. CONCLUSION

In this paper, a novel Lie group-based reliable IMM method was proposed for SINS/GNSS/OD/NHC integrated navigation in complex environments. Firstly, this method constructed a novel Lie group-based SSM to improve the estimation consistency of the subfilters, and further improves the OD/NHC model by using the proposed velocity-bias-based VB mounting error angle estimation method. Then, to address the state estimation instability caused by complex road environments,

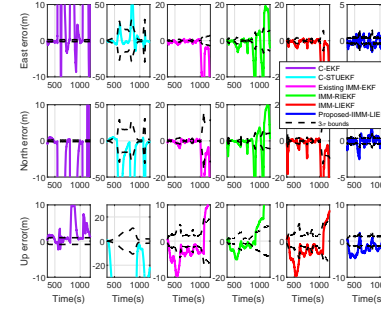


Fig. 24: 3σ bounds of the position error in the field test.

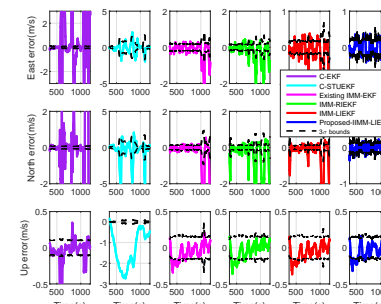


Fig. 25: 3σ bounds of the velocity error in the field test.

a DLAM-based model probability update method was introduced, which uses dynamic a weighted Gaussian and Student's t likelihood function value to mitigate negative impacts on filter performance. Finally, simulation and field test results

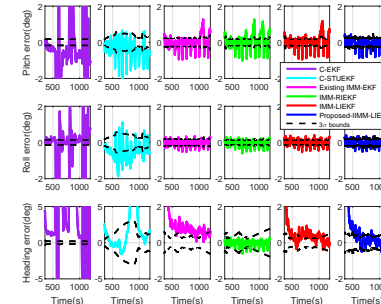


Fig. 26: 3σ bounds of the attitude error in the field test.

demonstrated that the proposed velocity-bias-based mounting error angle estimation method has better convergence speed and estimation accuracy. Additionally, in complex navigation environments, the proposed novel Lie group-based IMM estimation method also has higher accuracy and reliability compared with the existing IMM estimation methods.

REFERENCES

- [1] F. Yang, S. Wang, J. Li, Z. Liu, and Q. Sun, "An overview of Internet of Vehicles," *China Communications.*, vol. 11, no. 10, pp. 1-15, Oct. 2014.
- [2] S. Kuutti, S. Fallah, K. Katsaros, M. Dianati, F. McCullough, and A. Mouzakitis, "A survey of the state-of-the-art localization techniques and their potentials for autonomous vehicle applications," *IEEE Internet of Things Journal.*, vol. 5, no. 2, pp. 829-846, Apr. 2018.

- [3] N. Zhu, J. Marais, D. Bétaille, and M. Berbineau, "GNSS position integrity in urban environments: A review of literature," *IEEE Transactions on Intelligent Transportation Systems*, vol. 19, no. 9, pp. 2762-2778, Sep. 2018.
- [4] A. Abosekeen, A. Noureldin, M. Karamat, and C. Goodall, "A novel multi-level integrated navigation system for challenging GNSS environments," *IEEE Transactions on Intelligent Transportation Systems*, vol. 22, no. 8, pp. 4838-4852, Aug. 2020.
- [5] S. A. S. Mohamed, M.-H. Haghbayan, T. Westerlund, J. Heikkonen, H. Tenhunen, and J. Plosila, "A survey on odometry for autonomous navigation systems," *IEEE Access*, vol. 7, pp. 97466-97486, 2019.
- [6] M. Wang, W. Wu, X. He, Y. Li and X. Pan, "Consistent ST-EKF for Long Distance Land Vehicle Navigation Based on SINS/OD Integration," *IEEE Transactions on Vehicular Technology*, vol. 68, no. 11, pp. 10525-10534, Nov. 2019.
- [7] W. Ouyang, Y. Wu and H. Chen, "INS/Odometer Land Navigation by Accurate Measurement Modeling and Multiple-Model Adaptive Estimation," *IEEE Transactions on Aerospace and Electronic Systems*, vol. 57, no. 1, pp. 245-262, Feb. 2021.
- [8] R. Toledo-Moreo, M. A. Zamora-Izquierdo, B. Ubeda-Minarro, and A. F. Gomez-Skarmeta, "High-integrity IMM-EKF-based road vehicle navigation with low-cost GPS/SBAS/INS," *IEEE Transactions on Intelligent Transportation Systems*, vol. 8, no. 3, pp. 491-511, Sept. 2007.
- [9] K. Jo, K. Chu and M. Sunwoo, "Interacting Multiple Model Filter-Based Sensor Fusion of GPS With In-Vehicle Sensors for Real-Time Vehicle Positioning," *IEEE Transactions on Intelligent Transportation Systems*, vol. 13, no. 1, pp. 329-343, March 2012.
- [10] T. Zhang, K. Wu, J. Song, S. Huang, and G. Dissanayake, "Convergence and Consistency Analysis for a 3-D Invariant-EKF SLAM," *IEEE Robotics and Automation Letters*, vol. 2, no. 2, pp. 733-740, 2017.
- [11] M. P. Whittaker, and J. L. Crassidis, "Inertial navigation employing common frame error representations," in *AIAA Guidance, Navigation, and Control Conference*, USA, Jan. 2017.
- [12] M. P. Whittaker, and J. L. Crassidis, "Linearized analysis of inertial navigation employing common frame error representations," in *2018 AIAA Guidance, Navigation, and Control Conference*, USA, Jan. 2018.
- [13] M. Wang, W. Wu, P. Zhou, and X. He, "State transformation extended Kalman filter for GPS/SINS tightly coupled integration," *Gps Solutions*, vol. 22, no. 4, pp. 1-12, 2018.
- [14] A. Barrau, S. Bonnabel, "Invariant kalman filtering," *Annual Review of Control, Robotics, and Autonomous Systems*, vol. 1, pp. 237-257, 2018.
- [15] A. Barrau, "Non-linear state error based extended Kalman filters with applications to navigation," Diss. Mines Paristech, 2015.
- [16] R. Hartley, M. Ghaffari, R. M. Eustice, J. W. Grizzle, "Contact-aided invariant extended Kalman filtering for robot state estimation", *The International Journal of Robotics Research*, vol. 39, no. 4, pp. 402-430, 2020.
- [17] S. Heo and C. G. Park, "Consistent EKF-Based Visual-Inertial Odometry on Matrix Lie Group," *IEEE Sensors Journal*, vol. 18, no. 9, pp. 3780-3788, 2018.
- [18] S. Du, Y. Huang, W. Wen and Y. Zhang, "A Novel Consistent-Robust SINS/GNSS/NHC Integrated Navigation Method for Autonomous Vehicles Under Intermittent GNSS Outage," *IEEE Transactions on Intelligent Vehicles*, doi: 10.1109/TIV.2024.3406756.
- [19] L. Chang, F. Qin and J. Xu, "Strapdown Inertial Navigation System Initial Alignment Based on Group of Double Direct Spatial Isometries," *IEEE Sensors Journal*, vol. 22, no. 1, pp. 803-818, Jan. 1, 2022.
- [20] L. Chang, J. Di and F. Qin, "Inertial-Based Integration With Transformed INS Mechanization in Earth Frame," *IEEE/ASME Transactions on Mechatronics*, vol. 27, no. 3, pp. 1738-1749, June, 2022.
- [21] S. Du, F. Zhu, Z. Wang, Y. Huang and Y. Zhang, "A Novel Lie Group Framework-Based Student's *t* Robust Filter and its Application to INS/DVL Tightly Integrated Navigation," *IEEE Transactions on Instrumentation and Measurement*, vol. 73, pp. 1-21, 2024.
- [22] T. Cantelobre, C. Chahbazian, and A. Croux, "A real-time unscented Kalman filter on manifolds for challenging AUV navigation," *2020 IEEE/RSJ International Conference on Intelligent Robots and Systems*. USA, Oct, 2020.
- [23] S. Du, Y. Huang, B. Lin, J. Qian, and Y. Zhang, "A Lie Group Manifold-Based Nonlinear Estimation Algorithm and Its Application to Low-Accuracy SINS/GNSS Integrated Navigation," *IEEE Transactions on Instrumentation and Measurement*, vol. 71, pp. 1-27, 2022.
- [24] Y. Jin, W. -A. Zhang, J. Tang, H. Sun and L. Shi, "A Nonlinear Filter for Pose Estimation Based on Fast Unscented Transform on Lie Groups," *IEEE Robotics and Automation Letters*, vol. 9, no. 11, pp. 10431-10438, Nov. 2024.
- [25] L. Wang, X. Niu, T. Zhang, H. Tang, and Q. Chen, "Accuracy and robustness of ODO/NHC measurement models for wheeled robot positioning," *Measurement*, vol. 201, 111720, 2022.
- [26] E. Vinande, P. Axelrad, and D. Akos, "Mounting-angle estimation for personal navigation devices," *IEEE Transactions on Vehicular Technology*, vol. 59, no. 3, pp. 1129-1138, Mar. 2009.
- [27] Y. Wu, C. Goodall, and N. El-Sheimy, "Self-calibration for IMU/odometer land navigation: Simulation and test results," in *Proc. 2010 Int. Tech. Meeting Inst. Navigation*, 2010, pp. 652-659.
- [28] Q. Chen, Q. Zhang, and X. Niu, "Estimate the pitch and heading mounting angles of the IMU for land vehicular GNSS/INS integrated system," *IEEE Transactions on Intelligent Transportation Systems*, vol. 22, no. 10, pp. 6503-6515, Oct. 2020.
- [29] A. P. Sage and G. W. Husa, "Adaptive filtering with unknown prior statistics," in *Proc. Joint Autom. Control Conf.*, Boulder, CO, USA, 1969, pp. 760-769.
- [30] C. Hide T. Moore and M. Smith "Adaptive Kalman filtering for low-cost INS/GPS" *J. Navig.* vol. 56 no. 1 pp. 143-152 Jan. 2003.
- [31] Q. Xia M. Rao Y. Ying and X. Shen "Adaptive fading Kalman filter with an application" *Automatica* vol. 30 no. 8 pp. 1333-1338 Aug. 1994.
- [32] P. J. Huber, *Robust Statistics*, New York:Wiley 1981.
- [33] B. Chen, X. Liu, H. Zhao, and J. C. Principe, "Maximum correntropy Kalman filter," *Automatica*, vol. 76, no. 2, pp. 70-77, Feb. 2017.
- [34] Y. Huang, Y. Zhang, Z. Wu, N. Li, and J. Chambers, "A novel adaptive Kalman filter with inaccurate process and measurement noise covariance matrices," *IEEE Transactions on Automatic Control*, vol. 63, no. 2, pp. 594-601, Feb. 2018.
- [35] Y. Huang, Y. Zhang, N. Li, Z. Wu, and J. A. Chambers, "A novel robust Student's *t*-based Kalman filter," *IEEE Transactions on Aerospace and Electronic Systems*, vol. 53, no. 3, pp. 1545-1554, Jun. 2017.
- [36] Y. Huang, Y. Zhang, Y. Zhao, and J. A. Chambers, "A novel robust Gaussian-Student's *t* mixture distribution based Kalman filter," *IEEE Transactions on Signal Processing*, vol. 67, no. 13, pp. 3606-3620, Jul. 1, 2019.
- [37] Y. Yao, X. Xu, D. Yang, and X. Xu, "An IMM-UKF Aided SINS/USBL Calibration Solution for Underwater Vehicles," *IEEE Transactions on Vehicular Technology*, vol. 69, no. 4, pp. 3740-3747, Apr. 2020.
- [38] Q. Xu, L. Xu, and C.-Y. Chan, "Enhancing localization accuracy of MEMS-INS/GPS/in-vehicle sensors integration during GPS outages," *IEEE Transactions on Instrumentation and Measurement*, vol. 67, no. 8, pp. 1966-1978, Aug. 2018.
- [39] J. Xiong, J. W. Cheong, Z. Xiong, A. G. Dempster, S. Tian, and R. Wang, "Adaptive Hybrid Robust Filter for Multi-Sensor Relative Navigation System," *IEEE Transactions on Intelligent Transportation Systems*, vol. 23, no. 8, pp. 11026-11040, Aug. 2022.
- [40] G. Wang, X. Wang, and Y. Zhang, "Variational Bayesian IMM-Filter for JMSs With Unknown Noise Covariances," *IEEE Transactions on Aerospace and Electronic Systems*, vol. 56, no. 2, pp. 1652-1661, Apr. 2020.
- [41] C. Chen, W. Zhou, and L. Gao, "A novel robust IMM filter for jump Markov systems with heavy-tailed process and measurement noises," *Digital Signal Processing*, vol. 136, pp. 104003, 2023.
- [42] W. Youn, Y. Huang, and H. Myung, "Robust Localization Using IMM Filter Based on Skew Gaussian-Gamma Mixture Distribution in Mixed LOS/NLOS Condition," *IEEE Transactions on Instrumentation and Measurement*, vol. 69, no. 7, pp. 5166-5182, July. 2020.
- [43] D. Xu, Z. Wu, and Y. Huang, "A new adaptive Kalman filter with inaccurate noise statistics," *Circuits, Systems, and Signal Processing*, vol. 38, no. 12, pp. 4380-4404, 2019.
- [44] P. D. Groves, *Principles of GNSS Inertial and Multisensor Integrated Navigation Systems*. Norwood, MA, USA: Artech House, 2013.
- [45] H. A. P. Blom and Y. Bar-Shalom, "The interacting multiple model algorithm for systems with Markovian switching coefficients," *IEEE Transactions on Automatic Control*, vol. 33, no. 8, pp. 780-783, Aug. 1988.
- [46] Y. Bar-Shalom, X. R. Li and T. Kirubarajan, *Estimation with Applications to Tracking and Navigation: Theory Algorithms and Software*, John Wiley&Sons, 2001.
- [47] PSINS. Available: <http://www.psins.org.cn/sy>. Accessed on: Aug 26, 2024.



Siyuan Du received the B.S. and M.S. degrees in measurement and control technology and instruments from the School Instrument and Electronics, North University of China, Taiyuan, China, in 2015 and 2018, respectively. He is currently pursuing the Ph.D. degree in Automation from the Department of Intelligent Science and Engineering, Harbin Engineering University. His research interests include inertial navigation, integrated navigation, and information fusion.



Weisong Wen (Member, IEEE) received a BEng degree in Mechanical Engineering from Beijing Information Science and Technology University (BISTU), Beijing, China, in 2015, and an MEng degree in Mechanical Engineering from the China Agricultural University, in 2017. After that, he received a PhD degree in Mechanical Engineering from The Hong Kong Polytechnic University (PolyU), in 2020. He was also a visiting PhD student with the Faculty of Engineering, University of California, Berkeley (UC Berkeley) in 2018. Before joining PolyU as an

Assistant Professor in 2023, he was a Research Assistant Professor at AAE of PolyU since 2021. He has published 30 SCI papers and 40 conference papers in the field of GNSS (ION GNSS+) and navigation for Robotic systems (IEEE ICRA, IEEE ITSC), such as autonomous driving vehicles. He won the innovation award from TechConnect 2021, the Best Presentation Award from the Institute of Navigation (ION) in 2020, and the First Prize in Hong Kong Section in Qianhai-Guangdong-Macao Youth Innovation and Entrepreneurship Competition in 2019 based on his research achievements in 3D LiDAR aided GNSS positioning for robotics navigation in urban canyons. The developed 3D LiDAR-aided GNSS positioning method has been reported by top magazines such as Inside GNSS and has attracted industry recognition with remarkable knowledge transfer.



Yulong Huang (M'19-SM'24) received the B.S. degree in Automation from the College of Automation, Harbin Engineering University, Harbin, China, in 2012. He received the Ph.D. degree in control science and engineering from the College of Automation, Harbin Engineering University, Harbin, China, in 2018. From Nov. 2016 to Nov. 2017, he was a visiting graduate researcher at the Electrical Engineering Department of Columbia University, New York, USA. From Dec. 2019 to Dec. 2021, he was associated with the Department of Mechanical

Engineering, City University of Hong Kong, as a Hong Kong Scholar.

He is a Full Professor of navigation, guidance, and control, and Vice Dean of College of Intelligent Systems Science and Engineering at Harbin Engineering University (HEU) in China. His current research interests include state estimation, intelligent information fusion and their applications in navigation technology, such as inertial navigation, integrated navigation, intelligent navigation, and cooperative navigation. Currently, he serves as an Associate Editor for the IEEE TRANSACTIONS ON AEROSPACE AND ELECTRONIC SYSTEMS, for the IEEE TRANSACTIONS ON INSTRUMENTATION AND MEASUREMENT, and for the IEEE SENSORS JOURNAL, and a Youth Editor for the IEEE/CAA JOURNAL OF AUTOMATICA SINICA (JAS), for the JOURNAL OF MARINE SCIENCE AND APPLICATION, for the UNMANNED SYSTEMS TECHNOLOGY, for the JOURNAL OF UNMANNED UNDERSEA SYSTEMS, for the NAVIGATION POSITIONING AND TIMING.

He was the recipient of the 2018 IEEE Barry Carlton Award from IEEE TRANSACTIONS ON AEROSPACE AND ELECTRONIC SYSTEMS in 2022, the Honorable Mention of 2017 IEEE Barry Carlton Award from IEEE TRANSACTIONS ON AEROSPACE AND ELECTRONIC SYSTEMS in 2021, the Best Student Paper Award of 2023 IEEE International Conference on Mechatronics and Automation (IEEE ICMA 2023), and the Best Paper Award of 2021 International Conference on Autonomous Unmanned Systems (ICAUS 2021). He was also the recipient of the 11th China Youth Science and Technology Innovation Awards in 2018, the excellent doctoral thesis from Chinese Association of Automation (CAA) in 2019, the Wu Wen-Jun AI Excellent Youth Scholar Award in 2021, the First Prize of Natural Science Award of Chinese Association of Automation (Ranked the 2nd) in 2021, and he was selected into the sixth Young Elite Scientists Sponsorship Program by China Association for Science and Technology in 2020. He was an outstanding Associate Editor and Reviewer for the IEEE TRANSACTIONS ON INSTRUMENTATION AND MEASUREMENT.



Yonggang Zhang (S'06-M'07-SM'16) received the B.S. and M.S. degrees from the Department of Automation, Harbin Engineering University, Harbin, China, in 2002 and 2004, respectively. He received his Ph.D. degree in Electronic Engineering from Cardiff University, UK in 2007 and worked as a Post-Doctoral Fellow at Loughborough University, UK from 2007 to 2008 in the area of adaptive signal processing. Currently, he is a Professor of navigation, guidance, and control in Harbin Engineering University (HEU) in China. His current research interests include signal processing, information fusion and their applications in navigation technology, such as fiber optical gyroscope, inertial navigation and integrated navigation.